Tectonophysics 644–645 (2015) 122–137

Contents lists available at ScienceDirect

Tectonophysics

journal homepage: www.elsevier.com/locate/tecto

Magnetostratigraphic record of the early evolution of the southwestern Tian Shan foreland basin (Ulugqat area), interactions with Pamir indentation and India–Asia collision

Wei Yang [a,b,c,d,*], Guillaume Dupont-Nivet [c,d,e,f], Marc Jolivet [c], Zhaojie Guo [d], Laurie Bougeois [c], Roderic Bosboom [e], Ziya Zhang [d], Bei Zhu [d], Gloria Heilbronn [c]

[a] State Key Laboratory of Petroleum Resources and Prospecting, China University of Petroleum, Beijing 102249, China
[b] Unconventional Natural Gas Institute, China University of Petroleum, Beijing 102249, China
[c] Géosciences Rennes, Université Rennes 1, UMR 6118, CNRS/INSU, Rennes, France
[d] Key Laboratory of Orogenic Belts and Crustal Evolution, Ministry of Education, School of Earth and Space Sciences, Peking University, Beijing 100871, China
[e] Faculty of Geosciences, Utrecht University, The Netherlands
[f] Institute of Earth and Environmental Science, Potsdam University, Karl-Liebknecht-Str. 24-25, Golm, 14476 Potsdam, Germany

ARTICLE INFO

Article history:
Received 8 August 2014
Received in revised form 6 January 2015
Accepted 10 January 2015
Available online 24 January 2015

Keywords:
Magnetostratigraphy
Cenozoic
Tian Shan
Pamir
Tarim Basin
Tectonics

ABSTRACT

The Tian Shan range is an inherited intracontinental structure reactivated by the far-field effects of the India–Asia collision. A growing body of thermochronology and magnetostratigraphy datasets shows that the range grew through several tectonic pulses since ~25 Ma, however the early Cenozoic history remains poorly constrained. The time-lag between the Eocene India–Asia collision and the Miocene onset of Tian Shan exhumation is particularly enigmatic. This peculiar period is potentially recorded along the southwestern Tian Shan piedmont. There, late Eocene marine deposits of the proto-Paratethys epicontinental sea transition to continental foreland basin sediments of unknown age were recently dated. We provide magnetostratigraphic dating of these continental sediments from the 1700-m-thick Mine section integrated with previously published detrital apatite fission track and U/Pb zircon ages. The most likely correlation to the geomagnetic polarity time scale indicates an age span from 20.8 to 13.3 Ma with a marked increase in accumulation rates at 19–18 Ma. This implies that the entire Oligocene period is missing between the last marine and first continental sediments, as suggested by previous southwestern Tian Shan results. This differs from the southwestern Tarim basin where Eocene marine deposits are continuously overlain by late Eocene–Oligocene continental sediments. This supports a simple evolution model of the western Tarim basin with Eocene–Oligocene foreland basin activation to the south related to northward thrusting of the Kunlun Shan, followed by early Miocene activation of northern foreland basin related to overthrusting of the south Tian Shan. Our data also support southward propagation of the Tian Shan piedmont from 20 to 18 Ma that may relate to motion on the Talas Fergana Fault. The coeval activation of a major right-lateral strike-slip system allowing indentation of the Pamir Salient into the Tarim basin, suggests far-field deformation from the India–Asia collision zone affected the Tian Shan and the Talas Fergana fault by early Miocene.

1. Introduction

The Tian Shan is a 2500-km-long, up to 7400-m-high range extending through western China, Kazakhstan, and Kyrgyzstan. This range belongs to the larger Central Asian Orogenic Belt (CAOB) extending from the Urals to the Pacific across the East European, Siberian, North China, and Tarim cratons (e.g. Jolivet et al., 2010; Şengör et al., 1993; Windley et al., 2007). Cenozoic tectonic deformation of the Tian Shan is predominantly attributed to tectonic rejuvenation in response to the far-field effects of the India–Asia collision (e.g. Avouac et al., 1993; Huang et al., 2010; Patriat and Achache, 1984; Sun et al., 2009; Tapponnier et al., 2001; Van Hinsbergen et al., 2011; Yin et al., 1998). Thick Cenozoic accumulations of sediments derived mostly from the uplifting mountain range form the terrigenous depositional sequences that are well preserved and exposed in foreland basins of the Tian Shan (Charreau et al., 2009; Fang et al., 2005, 2006; Hendrix, 2000; Wu et al., 2006; Yang et al., 2013). The Tian Shan has provided an ideal setting for understanding Cenozoic intracontinental deformation in central Asia and the associated effects on regional environment and global climate. However, vigorous debate and gaps in understanding still exist concerning the Cenozoic history and driving mechanism of the Tian Shan orogeny arising mainly from the lack of accurate constraints on the exact time of deformation, uplift, and associated deposition. In particular, the early Cenozoic history of the range is poorly constrained. While the onset of exhumation is fairly well constrained

* Corresponding author. Tel./fax: +86 10 89739068.
E-mail address: yangw@pku.edu.cn (W. Yang).

http://dx.doi.org/10.1016/j.tecto.2015.01.003
0040-1951/

to have occurred at around the Oligo-Miocene boundary, it remains unclear what happened before that and why deformation accelerated only in the Middle to Late Miocene. More fundamentally, it remains unresolved why deformation from the India–Asia collision starting in the Eocene (ca. 50 Ma) propagated to the Tian Shan only in the early Miocene over 25 Myrs later.

Apatite fission track analyses from basement and sediments in the Tian Shan, as well as its piedmonts, predominately suggest an initiation of rapid uplift at ~25–20 Ma (e.g. Amidon and Hynek, 2010; Dumitru et al., 2001; Hendrix et al., 1994; Sobel and Dumitru, 1997; Sobel et al., 2006). Furthermore, Bullen et al. (2001, 2003) demonstrated that exhumation of the Kyrgyz Tian Shan continued at ~11 Ma, and younger exhumation ages ranging between 6 and 8 Ma are also reported from the Chinese Southwest Tian Shan (e.g. Wang et al., 2010). Recent magnetostratigraphic studies have also been conducted on Cenozoic sediments from both the northern and southern piedmonts of the Tian Shan. Several main pulses in increased sedimentation rate were detected, reflecting the multi-phased uplift and deformation of the Tian Shan at ~26–23 Ma, ~17–16 Ma, ~13–11 Ma, ~7 Ma and ~4 Ma (e.g. Bullen et al., 2001; Charreau et al., 2005; Huang et al., 2006, 2010; Jin et al., 2008; Li et al., 2011; Lu et al., 2010; Sun et al., 2004, 2009). However, these studies have concentrated on the Miocene and later Tian Shan evolution focusing on correctly constraining the Cenozoic episodic uplift of the Tian Shan. What happened in the period between the Eocene India–Asia collision and the Miocene Tian Shan exhumation remains to be explored.

In that period, recent studies have focused on the record of the westward retreat of the vast epicontinental sea that covered the Tarim Basin at the eastern end of a shallow sea that formerly extended across the Eurasian continent (e.g. Bosboom et al., 2011; Garzione et al., 2005; Graham et al., 2005; Kent-Corson et al., 2009; Ramstein et al., 1997; Zhang et al., 2007). Accurate age estimates on the youngest marine sediments indicate final sea retreat from the northern Tarim basin in the late Eocene (Bosboom et al., 2014a). However, it remains unclear what happened between the deposition of these last marine deposits and the overlying continental deposits as the latter are virtually unconstrained in age. They have been usually attributed an Oligocene to Miocene age based mainly on the fact that they lie on marine sediments of Eocene age and are overlain by Miocene series.

In this paper, we report a detailed magnetostratigraphic study of such continental sediments at the Mine section located in the Ulugqat area in the piedmont of the Southwest Tian Shan (Fig. 1). This section has been chosen because it lies directly on dated marine deposits (Bosboom et al., 2014a) thus providing a basal age constraint and because it encompasses a complete and well developed sequence of the early continental deposits with a total thickness of ~1700 m. This section also has previously published detrital Apatite Fission Track (AFT) ages and detrital U/Pb zircons ages that provide additional age and provenance information (Yang et al., 2014).

2. Regional stratigraphic and geological setting

A series of representative forelands, characterized by well-preserved infillings of Cenozoic sediments, were deposited along the margins of the Pamir, western Kunlun and Southwest Chinese Tian Shan (SWTS), such as the Kuqa subbasin (e.g. Heermance et al., 2007; Li et al., 2004), the Fergana–Alai Basin (e.g. Burtman, 2000; De Grave et al., 2012), and the Afghan–Tadjik Basin (e.g. Thomas et al., 1994) from east to west. These basins are clearly related to significant Miocene deformation widely developed diachronously across these basins characterized by increasing accumulations rates recorded throughout Miocene times (Amidon and Hynek, 2010; Heermance et al., 2007; Li et al., 2011; Liao et al., 2012; Sobel and Dumitru, 1997; Sobel et al., 2006; Yin et al., 2002). Underlying these Miocene strata, poorly dated late Paleogene to early Neogene sediments are regionally extensive suggesting that they were part of a larger basin that was later segmented. Although age constraints are still lacking, these strata have been correlated regionally across basins from Central Asia based mainly on lithofacies and marine micro- and macro-fossil assemblages (Table 1; Bosboom et al., 2011, 2014a,b; Coutand et al., 2002; Jia et al., 2004). Due to this lack of age constraints it remains unclear whether these strata can be associated with an enigmatic Eocene–Oligocene regional tectonic phase or to the onset of the ensuing Miocene tectonism.

The study area is located at the junction of the Southwest Tian Shan to the north and the western Kunlun/northern Pamir to the south, whose tectonic evolution is summarized as follows.

To the north of the study area, the east–west trending Tian Shan extends through western China, Kazakhstan and Kyrgyzstan and represents an important part of the Central Asian Orogenic Belt (CAOB). The topographic evolution of the Tian Shan has been the focus of considerable attention leading to the interpretation that it formed during Late Cenozoic times as a result of the distant effects of the ongoing India–Eurasia collision (e.g. Avouac et al., 1993; Burchfiel and Royden, 1991; Burchfiel et al., 1999; Buslov et al., 2004, 2007; Dumitru et al., 2001; Jolivet et al., 2010; Molnar and Tapponnier, 1975; Tapponnier and Molnar, 1977; Wei et al., 2014; Yin et al., 1998). The Southwest Chinese Tian Shan (SWTS) is characterized by ~9 km of Cenozoic sediments accumulated in a foreland basin setting forming the northwestern part of the Tarim Basin (e.g. Chen et al., 2002; Heermance et al., 2007). Cenozoic deformation, shortening, and uplift in the SWTS and its piedmonts are interpreted to have commenced at ~25–20 Ma, as indicated by significant exhumation around the Oligocene–Miocene boundary (e.g. Hendrix et al., 1994; Ji et al., 2008; Sobel, 1995; Sobel and Dumitru, 1997; Sobel et al., 2006; Yin et al., 1998). Subsequently, renewed exhumation at 19 ± 3 Ma is reported in the SWTS (Heermance et al., 2007; Sobel et al., 2006) and a southward propagation of deformation indicated by diachronous deposition of alluvial fan conglomerates and several abrupt increases in accumulation rates respectively at ~16, 13 Ma, and 4 Ma (Heermance et al., 2007; Li et al., 2011). To the south of the study area is the eastern limb of the Pamir salient orogenic belt. It is also referred as the western Kunlun Shan and extends from the northern margin of the Tibetan Plateau to the south to the Tian Shan along the southwestern margin of the Tarim Basin. The timing of indentation of the Pamir salient, and in particular its relation with the Tian Shan, remains poorly understood, and has important implications on Paratethys sea retreat, Asian climate and tectonism (e.g. Bosboom et al., 2011, 2014a,b,c; Sobel et al., 2013). It is generally assumed that the far-field effects of the India–Eurasia collision induced multiple stages of uplift and erosion during the Cenozoic within the western Kunlun and Pamir (Amidon and Hynek, 2010; Burtman and Molnar, 1993; Cui et al., 2006; Jolivet et al., 2001; Liu et al., 2010; Sobel and Dumitru, 1997; Sobel et al., 2011, 2013; Wang et al., 2006). Sobel and Dumitru (1997) and Yin et al. (2002) initially suggested that strong exhumation and cooling occurred during the latest Oligocene to Middle Miocene, based on sedimentary facies, provenance changes, and thermochronological data from the southwestern Tarim Basin. Recent thermochronological data results suggest a more complex exhumation and deformation pattern, divided into three stages: the Late Oligocene to Early Miocene (Cao et al., 2009; Li et al., 2007; Liu et al., 2010), the Middle to Late Miocene (Cao et al., 2009; Liu et al., 2010; Wang et al., 1999, 2001, 2002) and the Late Miocene to present day (e.g. Cao et al., 2009; Li et al., 2005, 2007; Liu et al., 2010). Additionally, the interaction between the Pamir and the SWTS changed the sedimentation and drainage patterns (Zheng et al., 2006). The onset of this change has been recently estimated as Oligocene–Miocene by provenance and thermochronological data but still remains poorly constrained in the sedimentary record (e.g. Cao et al., 2013; Sobel et al., 2011).

3. Age constraints from biostratigraphy

In the study area, Cenozoic strata exposed in the western Tarim consist of: 1) the Kashi Group, which comprises in chronological order the

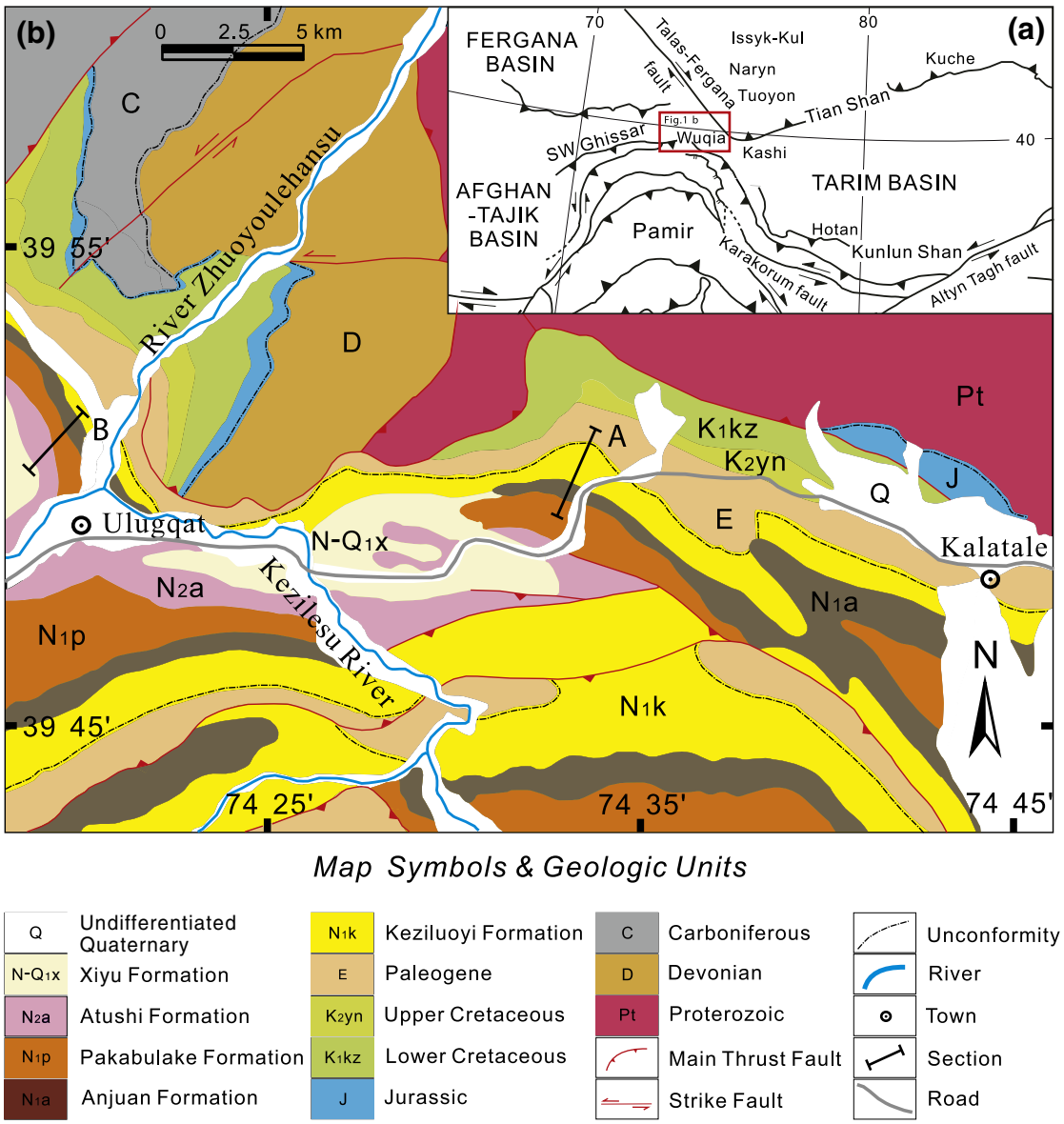

Fig. 1. (a) Location of the study area shown on large-scale map displaying major tectonic features. (b) Simplified geological map of the Ulugqat area with location of the Mine (A) and Ulugqat (B) sections.

Aertashi, Qimugen, Kalatar, Wulagen and Bashibulake Formations (e.g. Bosboom et al., 2011; Jia et al., 2004; Mao and Norris, 1988) (Figs. 1 and 2); 2) the overlying continental Wuqia Group which consists of the Kezilouyi, Anjuan and Pakabulake Formations (Table 1); 3) the overlying Atushi Formation; and 4) the Xiyu Formation characterized by typical conglomerates. A summary of the observed and published descriptions of lithologies and depositional systems is presented below with a summary review of the existing age determinations (Jia et al., 2004).

The marine Bashibulake Formation, which is at the top of the Kashi Group, is characterized by littoral and neritic deposits yielding dinoflagellates, nannoplankton, foraminifers, ostracods and bivalves. The Bashibulake Formation corresponding to the fifth and last sea retreat from the westernmost Tarim has been assigned a Late Eocene depositional age ranging between ~38.5 and 35.5 Ma by recent biostratigraphic analysis (Bosboom et al., 2014a; Jia et al., 2004; Lan, 1997; Lan and Wei, 1995; Mao and Norris, 1988; Yang et al., 1995). However, the overlying continental strata are poorly constrained in age.

At the base of the Wuqia group, the Keziluoyi Formation overlies disconformably or locally with a slight angular unconformity the Bashibulake Formation (BGMRXUAR, 1993; Jia et al., 2004). It consists largely of fluvio-lacustrine facies (e.g. Jia et al., 2004; Tang et al., 1989). It contains foraminifers, ostracods, chareae and sporopollen. Although the presence of ostracods *Pontocyprismican* suggests a marine sedimentary environment, ostracods *Corycaeus speciosus* and *Hemicyprideis* indicate a fresh water sedimentary environment, supported by the appearance of Charophyta algae. Recovered poorly developed foraminifera fauna is indigenous and similar to the underlying Eocene Marine strata such that they do not provide age constraints (Hao et al., 2002). The Keziluoyi Formation was broadly assigned a Late Oligocene–Early Miocene age as it lies on top of the Bashibulake Formation previously assigned an Oligocene age which we show to be incorrect in this study (e.g. Gao et al., 2000; Lan, 1997; Lan and Wei, 1995; Yin et al., 2002; Zheng et al., 1999). The Keziluoyi Formation was further defined as belonging to the Xiejian stage of the continental Miocene series in China (early to middle Aquitanian age from ~23.0 to 21.0 Ma according to

Table 1
Simplified litho-biostratigraphic correlation of the Kuqa subbasin, Fergana–Alai and Afghan–Tadjik Basins to the chronological framework recognized in the southwest Tarim Basin.

Age (Ma)		Afghan–Tadjik Basin	Fergana–Alai Basin	Kuqa subbasin (Northern Tarim)	Western Tarim Basin
Neogene	Miocene	Tavildara Formation Hingou Formation Childara Formation	Sokh Formation Baktry Formation	Kangcun Formation Jidike Formation	Pakabulake Formation Anjuan Formation
		Baldzhua complex/Kamoli Formation	Massaget Formation	Suweiyi Formation	Keziluoyi Formation
Paleogene	Oligocene[a]	Shurysay Formation Hissarak Formation			Bashibulake Formation
	Late Eocene	Sanglak Formation	Shurysay Formation Sumsar Formation Hanabad Formation Isfara Formation Rishtan Formation		

Notes: We show here that the age of the Keziluoyi Formation is actually Miocene.
[a] Note to Table 1: The Keziluoyi Formation is dated here to the Miocene rather than Oligocene. The wavy line represents the hiatus between the Late Eocene and Miocene reported here. Review based on Bosboom et al. (2014a,b); Coutand et al. (2002); Dzhalilov et al. (1982); Jia et al. (2004); Pomazkov (1972).

GTS2012) based on a review of continental biostratigraphic evidence recovered from those strata (see Jia et al., 2004).

The Anjuan Formation conformably overlies the Keziluoyi Formation. The contact between these two formations is based on increased occurrences of siltstone and sandstone within brown-red mudstones to gray-green mudstones. The Anjuan Formation comprises dominantly fluvial to shallow lacustrine deposits but may include some marine intervals based on foraminifera assemblages (e.g. Jia et al., 2004; Tang

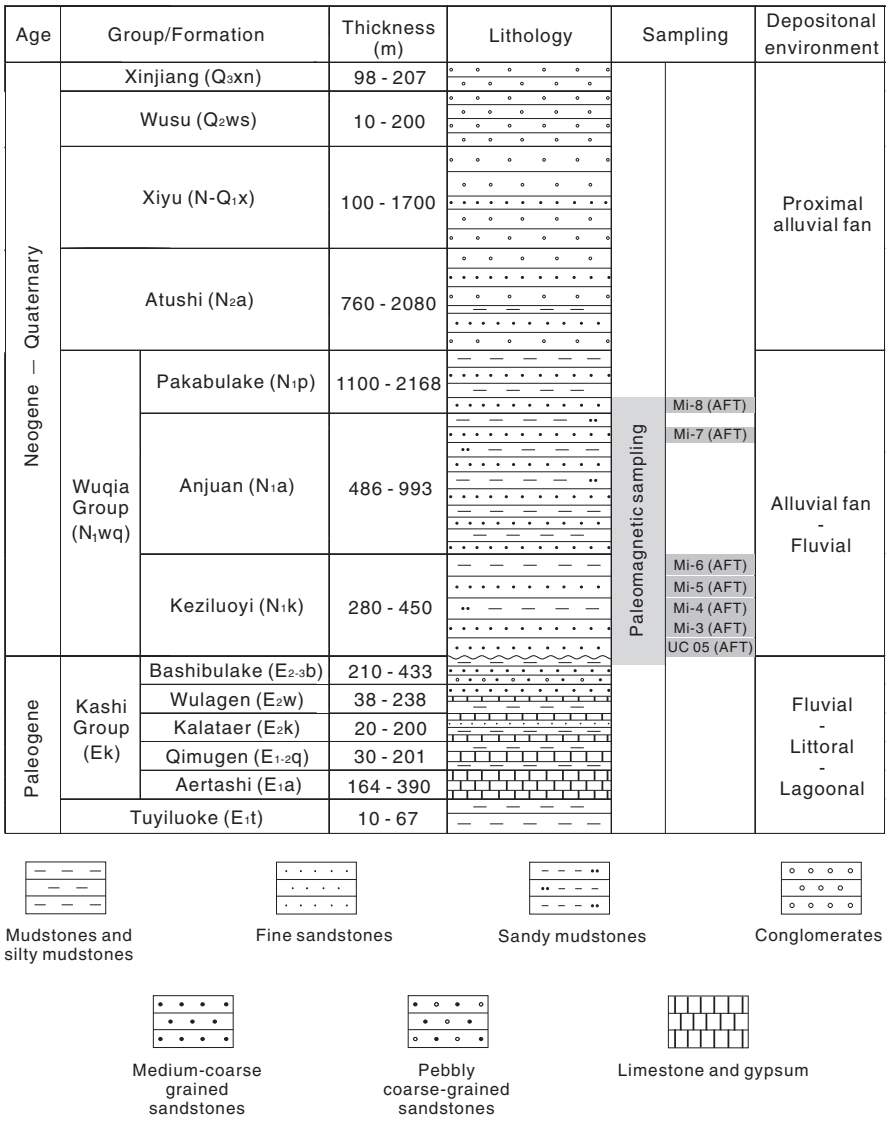

Fig. 2. Generalized stratigraphic column of the Cenozoic series of the studied Ulugqat area.
Modified after Yang et al., 2013.

et al., 1989). The Anjuan Formation contains foraminifers, ostracods, chareae and sporopollen. The presence of ostracods *Darwinula stevensoni*, *Limnocythere aligra*, *Cyclocypris* cf., *cavernosa*, *Limnocythere argulata*, and *Ilyocypris evidens* suggests a fresh water sedimentary environment, while ostracods *Cypinotus daductus* and *Leptocythere parva* respectively indicate fresh water to brackish environment. Additionally, the foraminifer association composed of *Ammonia honyaensis*, *Ammonia hatatatensis*, *Ammonia beccarii*, *Ammonia japonica*, *Ammonia limnetes*, *Ammonia multicella* and *Ammonia tepida* suggests a marine brackish water sedimentary environment, supported by the appearance of ostracods *Candona* sp., *Cyprinotus deformis*, *Ilyocypris errabundis*, *Hemicyprinotus valvaetumidus* and *Eucypris* sp., as well as foraminifers *Pararotalia armata*, *Cibicides borislavensis*, *Eponides* sp., *Nonion bogdanowiczi* and *Elphidium* sp. Based on these foraminifera, an Early to Middle Miocene age has been assigned to this formation (Hao et al., 2002) corresponding to the Shanwangia stage (late Aquitanian–Burdigalian from ~21.0 to 16.0 Ma GTS2012).

The Pakabulake Formation conformably overlies the Anjuan Formation. The contact is vaguely defined as the appearance of gray-green thick-bedded and massive sandstones within the stratigraphy dominated by red-brown to dark gray mudstones interbedded with sandy mudstones. The Pakabulake Formation is inferred to be fluvio–shore shallow lacustrine deposits (e.g. Jia et al., 2004; Tang et al., 1989). It contains foraminifers, ostracods, chareae and sporopollen. The Pakabulake Formation was assigned to the Tonggurian and Baodean stages (Langhian–Messinian from ~16.0 to 5.3 Ma GTS2012) based mainly on lithostratigraphic correlation and scarce and poorly constrained biostratigraphy (Gao et al., 2000; Jia et al., 2004; Zheng et al., 1999).

The Atushi Formation conformably overlies the Pakabulake Formation. It consists largely of reddish-gray conglomerates and sandstones interbedded with minor mudstones, and represents alluvial sedimentary environments (Bershaw et al., 2012; Jia et al., 2004). It contains ostracods *Ilyocypris manasensis*, *Darwinula* sp., *I. errabundis*, *Candona compresaformis*, *C.* spp., *Candoniella albicans*, *Eucypris* sp., *Candona neglecta*, *Candona irgizica*, *Candoniella kasachstanica*, *Candoniella aucta*, *Ilyocypris sincera*, *Eucypris notabilis*, chareae *Sphaerochara inconspicus*, as well as sporopollen *Laricoidites* sp. and *Graminidites* sp. (Jia et al., 2004). The overlying Xiyu Formation is characterized by typical gray conglomerates, interbedded with gray medium-grained litharenite and sandy mudstones, corresponding to alluvial fan deposits (Jia et al., 2004). The Atushi and Xiyu Formations were assigned late Neogene to Quaternary ages (the Gaozhuangian and Mazegouan stages), based mainly on recent magnetostratigraphic analyses indicating highly diachronous Middle to Quaternary onset of conglomeratic deposition following thrust propagation over the region (Charreau et al., 2009; Heermance et al., 2007).

4. Age constraints from apatite fission track analyses

Additional age constraints are provided by detrital apatite fission track (AFT) analyses on seven samples from the study area previously published in Yang et al. (2014). Six sandstone samples come directly from the studied magnetostratigraphic sequence in the Mine section (see Fig. 2; four samples from the Keziluoyi Formation, one from the Anjuan and one from the Pakabulake Formation, respectively). One more sandstone sample (UC05) collected from the Keziluoyi Formation in the adjacent Ulugqat section was also analyzed (Fig. 1; Yang et al., 2014). The 331 individual ages obtained from these samples vary from 18.2 ± 7.8 Ma to 134.4 ± 98.2 Ma. Yang et al. (2014) interpreted that the obtained AFT age populations in the Wuqia group have not been partially reset and can therefore be used to infer maximum depositional ages.

For the four Keziluoyi Formation samples (Mi-3, Mi-4, Mi-5 and Mi-6), the 232 individual grain ages obtained range from 25.6 ± 12.2 Ma to 111.8 ± 39.6 Ma. Mi-3 (35 meter-level) has the two youngest ages respectively at 26.3 and 26.9 Ma, Mi-4 (175 meter-level) has one youngest age at 27.1 Ma, and Mi-5 (370 meter-level) has three youngest ages respectively at 27.6, 27.8 and 27.8 Ma. Mi-6 (570 meter-level) provides the youngest and the largest cluster with four youngest ages (25.6 ± 12.2, 25.6 ± 12.2, 25.6 ± 13.7 and 25.6 ± 19.3 Ma, respectively) suggesting a maximum depositional age around 25 Ma.

For the Anjuan Formation sample collected around level 1075 (Mi-7), the 60 individual grain ages range from 18.2 ± 7.8 Ma to 87.6 ± 32.4 Ma, with the youngest two ages (18.2 ± 7.8 and 18.5 ± 9.8 Ma) interpreted as the maximum depositional age of this level. Finally for the Pakabulake Formation sample collected around level 1720 m (Mi-8), the 39 individual ages range between 20.9 ± 9.8 Ma and 134.4 ± 98.2 Ma suggesting a maximum depositional age within error relative to the underlying Anjuan Formation samples. The older maximum depositional age can be interpreted as reworking of the underlying sediments or a change within the drainage system (Yang et al., 2014).

5. Lithostratigraphy of the sampled section

Here we focus on the Mine section (39°51′N, 74°32′E; Section A on Fig. 1) situated at the western margin of the Tarim Basin (Fig. 1). The Mine section (named after a nearby recently active mine) is close or identical to the Bashibulake section which has been part of earlier biostratigraphic studies by Lan and Wei (1995), Lan (1997), Mao and Norris (1988) and Tang et al. (1989). The lower marine part belonging to the Bashibulake Formation has been previously described and dated with biostratigraphy as Priabonian (38.5–35.5 Ma, Bosboom et al., 2014a). Following on this previous work, the continental strata overlying these marine deposits are here described and dated using magnetostratigraphy. The strata are exposed continuously in a tributary valley with variable dipping attitudes through gentle folding but no significant faults. The stratigraphic thicknesses of the recognized lithostratigraphic units were measured to decimetric precision above the zero meter level defined by the last shell bed of the marine Bashibulake formation. A complete description of the Bashibulake Formation at the Mine section, available in Bosboom et al. (2014a), is summarized as follows. The Bashibulake Formation can be divided into five segments, and mainly composed of red-brown mudstones, sandy mudstones, orange and gray-green sandstones, pebbled sandstones, gypsum interbeds, and green-gray sandy limestone rich in bivalves. The first segment is mainly characterized by red-brown mudstones and siltstones, only containing foraminifers (Bosboom et al., 2014a; Jia et al., 2004). The lower part of the second segment mainly consists of red-brown silty mudstones containing foraminifers, bivalve, ostracods, dinoflagellate and sporopollen, while the upper part is predominantly characterized by gray-green silty mudstones containing scolites, foraminifers, ostracods, dinoflagellate, coccolith and sporopollen. The third segment of the Bashibulake Formation is mainly composed of gray-green mudstones and lumachelle containing gastropod, foraminifers, bivalve, ostracods, dinoflagellate, coccolith and sporopollen. The fourth segment mainly consists of dark purple mudstones interbedded with gray shell marl containing foraminifers, gastropods, bivalve, ostracods, chlorophyceae, coccolith, dinoflagellate and sporopollen. The fifth segment is again composed of red-brown mudstones and silty mudstones containing pebbles, foraminifers and ostracods (Bosboom et al., 2014a; Jia et al., 2004; Lan, 1997; Lan and Wei, 1995; Mao and Norris, 1988; Yang et al., 1995). The Bashibulake Formation is thus characterized by littoral and neritic deposits.

A low angle (<5°) unconformity is observed between the Keziluoyi Formation and the underlying Bashibulake Formation, characterized by a fine gravel conglomerate layer with a thickness of ~0.5 m (~15 m level). This gravel is directly overlain by tan sandstone beds with well-developed meter-scale trough-cross-bedding. The lower unit of the Keziluoyi Formation mainly consists of red-brown mudstones interbedded with gray-green silty mudstones, argillaceous sandstones and

siltstones. The upper unit is dominated by red-brown and purple-red mudstones, irregularly interbedded with gray-green thin-bedded massive sandstones and thin-bedded siltstones and occasional laminated gypsum. The lithological associations between dark mudstones and gray-green sandstones above are indicative of a fluvio-lacustrine environment (Fig. 3). The Keziluoyi Formation covers a total thickness of ~570 m.

The Anjuan Formation conformably overlies the Keziluoyi Formation with a relatively gradual transition such that the boundary is poorly constrained (~585 m level) (Fig. 3). The basal unit in the Anjuan Formation consists dominantly of brown and more regular occurrences of gray-green fine-medium sandstones with trough-cross-bedding. Interbedding of medium-thick bedded medium-grained sandstones and brown mudstones, characterizes the next unit of the Anjuan Formation. Upward, brown mudstones and thin-bedded fine-grained sandstones are present as intercalated beds in the third unit, while brown and gray-green thick-bedded sandstones are dominant in the top unit interbedded with dark brown mudstones and carbonaceous black mudstones. The lithological associations dominated by medium-thick bedded sandstones above are interpreted as shallow lacustrine deposits, and a general coarsening upward sequence can be recognized in the Anjuan Formation with beds getting thicker (10-meter thick). Well-developed lenticular fluvial beds are present, indicating a meandering system with overbank deposits. The Anjuan Formation spans ~723 m in thickness.

The Pakabulake Formation conformably overlies the Anjuan Formation. It is defined by the first occurrence (~1308 m level) of bedded gray conglomerates and conglomeratic sandstones within red-brown mudstones to sandstones that constitute the basal unit. The second unit consists dominantly of brown poorly sorted pebbly sandstones interbedded with red-brown siltstones characterized by braided channels (Fig. 3). The studied sequence from the Pakabulake Formation covers ~419 m in thickness reaching the top of the measured section (39°50′N, 74°33′E). The section above is discontinuous in outcrop such that it was not logged nor sampled for magnetostratigraphy. The overlying Atushi Formation mainly consists of reddish brown conglomerates and sandstones interbedded with minor mudstones, and represents alluvial sedimentary environments (Bershaw et al., 2012; Jia et al., 2004). Finally, the contact with the overlying conglomeratic Xiyu Formation could be clearly distinguished and is estimated to occur stratigraphically ca. 1400 m above the top of the measured section.

6. Magnetostratigraphy

Paleomagnetic sampling at the Mine sections was performed using a portable electric drill powered by a portable gasoline generator. 541

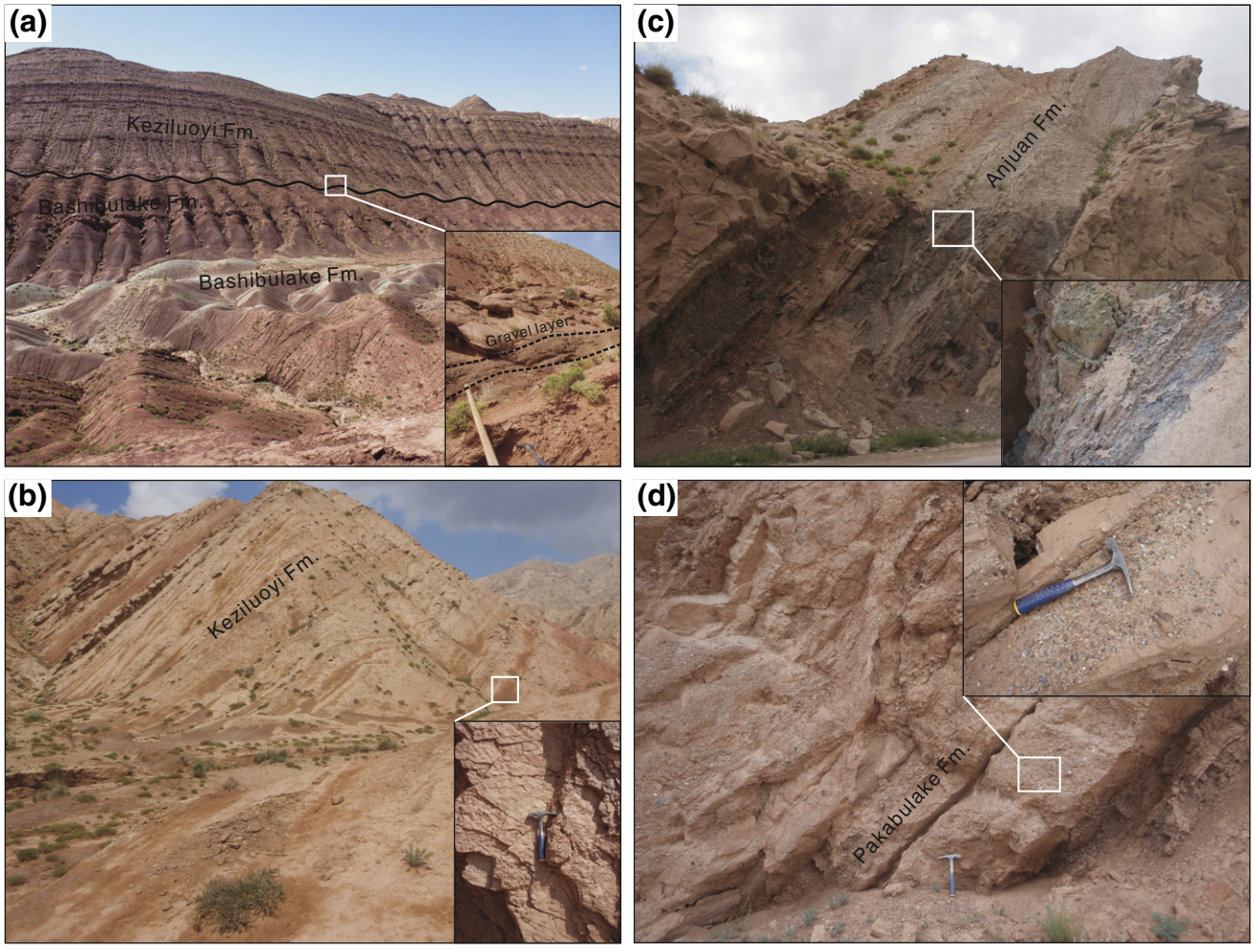

Fig. 3. Field photographs of formations and sedimentological features at the Mine section. (a) Angular unconformity between the Bashibulake and Keziluoyi Formation, channel sandstone beds of the Bashibulake Formation indicative of a fluvial depositional environment, and the gravel layer at the bottom of the Keziluoyi Formation. (b) Red mudstones interbedded with thick-bedded sandstones of the upper part of the Keziluoyi Formation indicative of the fluvio-lacustrine facies. Sinuous-crested ripples are locally developed. (c) Brown-red mudstones interbedded with gray-green mudstones, siltstones and sandstones of the Anjuan Formation indicative of a fluvio-lacustrine environment. (d) Conglomeratic sandstones, occasional red-brown mudstones and sandy mudstones of the basal unit of the Pakabulake Formation indicative of fluvial to alluvial fan deposits, with a thin-bedded gravel layer present at the bottom.

samples were collected at an average 4-meter resolution (intervals ranging from 0.2 to 22.8 m) through the continuous Mine section ranging from the uppermost Bashibulake, through the Keziluoyi, Anjuan and Pakabulake formations described above. A broad fold within the section enabled us to sample for a paleomagnetic fold test in order to check the reliability of the Characteristic Remanent Magnetization. Samples were orientated with a standard magnetic compass. After fieldwork, samples were cut into core specimens of approximately 2 cm in length for further paleomagnetic analyses.

6.1. Rock magnetism and thermal demagnetization

Within the shielded room of the paleomagnetic Laboratory of the Faculty of Geosciences at the Université de Rennes 1, specimens were thermally demagnetized in a shielded oven (MMTD80) by using up to 21 temperature steps varying between room temperature (~25 °C) and 690 °C with intervals of 50 °C up to 550 °C, of 25 °C from 550 to 650 °C, of 10 °C from 650 to 670 °C, and of 5 °C from 670 to 690 °C. Natural Remanent Magnetizations (NRMs) of samples were measured on a 2G Enterprises DC SQUID cryogenic magnetometer housed in the shielded room. To monitor mineral changes upon heating, bulk magnetic susceptibility was measured for each sample between each step on a Bartington MS2 magnetic susceptibility meter. Demagnetization behaviors varied with lithologies and can be distinguished into three main groups as follows.

The first group (Group A) includes most samples of the marine red sediments of the Bashibulake Formation. These samples are characterized by low initial NRM intensities on the order of 10^{-4} A/m that are demagnetized mainly below 450–500 °C with demagnetization paths generally towards the origin (Fig. 4). After 450–500 °C NRM intensities and bulk susceptibilities strongly increase and the demagnetization path becomes erratic. These properties are similar to properties obtained from the red marine deposits of the Wulagen Formation collected at the Aertashi and Mine sections of the southwestern Tarim basin (Bosboom et al., 2014a, b) where they were interpreted as resulting from the combination of magnetite and iron sulfides; the latter undergoing mineral transformation upon laboratory heating.

The second group (Group B) was observed in most of the samples. It includes mostly finer grained sandstones from the continental red beds of the overlying Wuqia group (Keziluoyi, Anjuan and Pakabulake

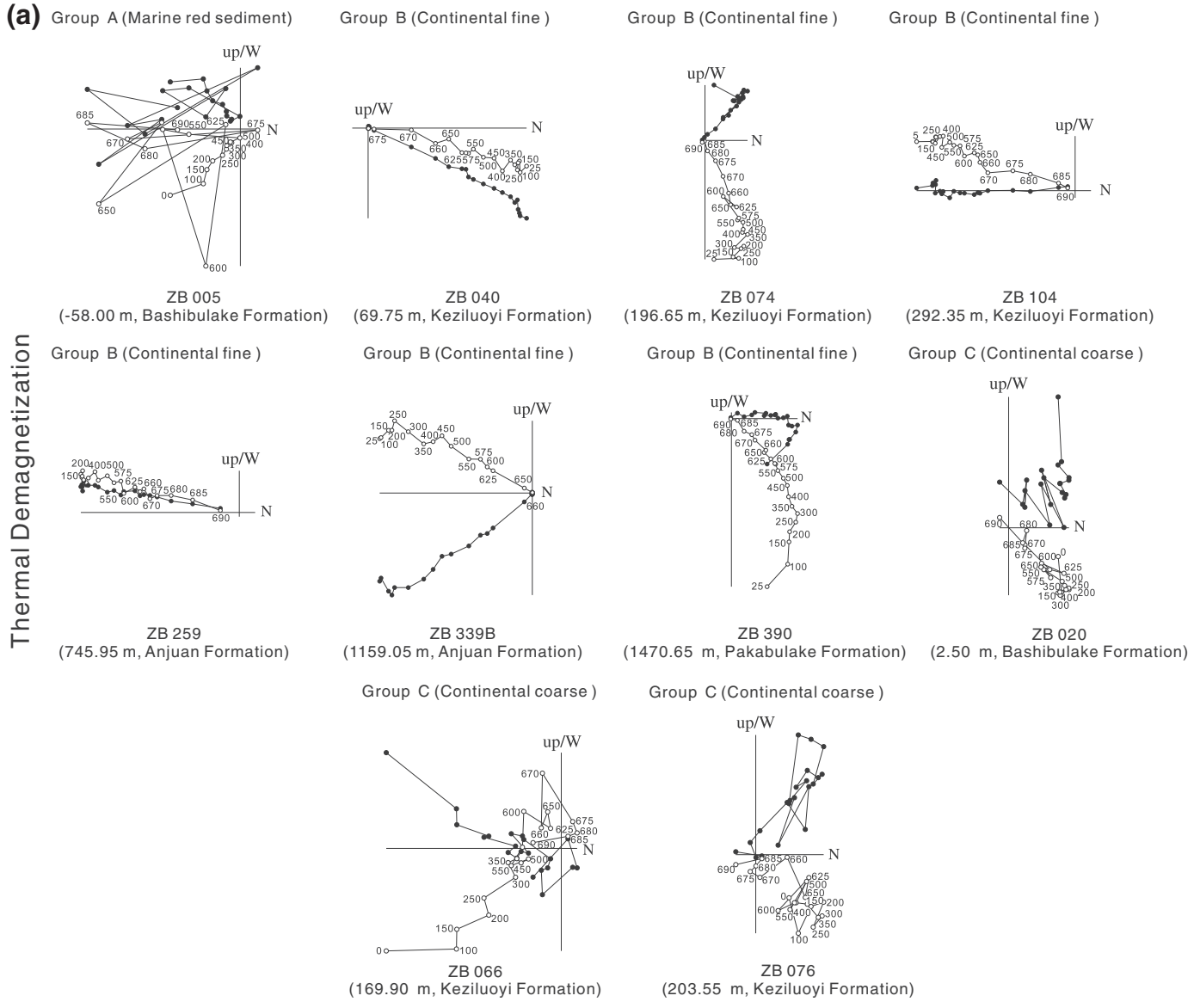

Fig. 4. (a) Plots showing typical thermal demagnetization behaviors of representative specimens of Groups A, B and C with Quality 1, 2 and 3 (see text). Full (open) symbols are projections on the horizontal (vertical) plane. Numbers next to symbols indicate temperature of demagnetization steps in °C. (b) Associated behavior of bulk susceptibility (SI) and (c) NRM intensity (10^{-5} A/m).

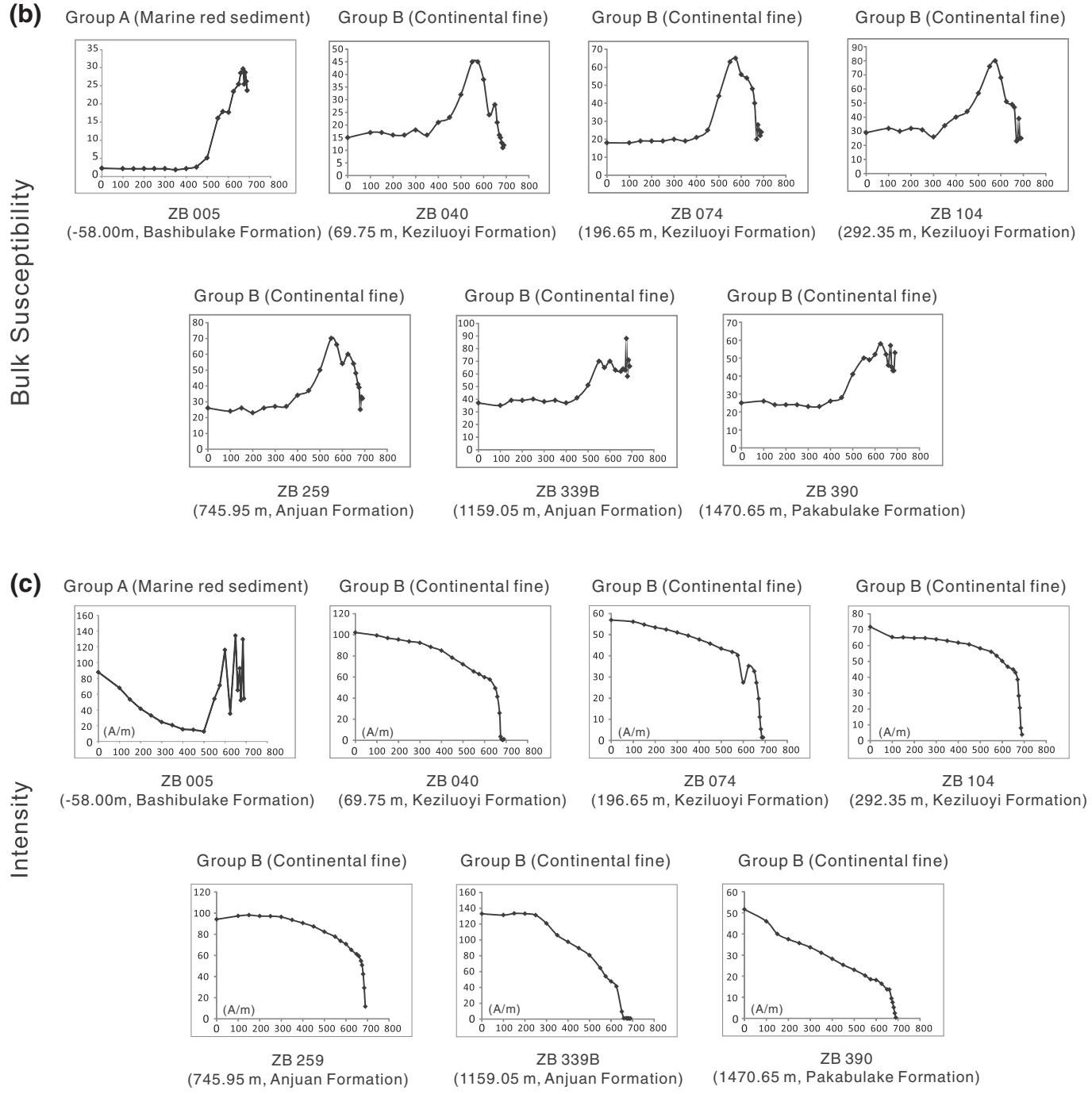

Fig. 4 (*continued*).

Formations). These display higher initial intensities on the order of 10^{-3} A/m. A Low Temperature Component (LTC) in the normal present day field direction representing usually only a small portion of the NRM is demagnetized from room temperature to below 250 to 400 °C. Most of the NRM is constituted by an Intermediate Temperature Component demagnetized from 250–400 °C up to 600–650 °C and a High temperature Component from 600–650 °C to 660–690 °C. In this group the ITC and the HTC were defined as the Characteristic Remanent Magnetizations (ChRMs) as they generally have the same directions and decay linearly towards the origin. They are interpreted to represent a combination of magnetite and hematite.

The third group (Group C) includes mostly coarser grained sandstones from the continental red beds of the overlying Wuqia group (Keziluoyi, Anjuan and Pakabulake Formations). They display low initial intensities on the order of 10^{-4} A/m. Demagnetization behaviors are similar to the ones of Group B except that the demagnetization path is erratically decaying towards the origin. The LTC and ITC are often overlapping and difficult to separate and the HTC is often not distinguishable. An increase in the susceptibility at around 350 °C followed by a later decrease suggests the additional presence of maghemite in these coarser lithologies more prone to alteration.

6.2. ChRM direction analyses

The ChRM directions were determined by principal component analysis thermal demagnetization diagrams (Kirschvink, 1980) on a

minimum of four main successive steps without anchoring the line-fit to the origin, except for some highly erratic demagnetization paths of Groups A and C. Maximum angular deviations (MADs) on the line-fits were usually below 15°, but MADs of up to 30° were accepted if the polarity could be clearly discerned. In total, 478 ChRM directions in all were obtained from the 541 collected samples. These ChRM directions are separated into 'Quality 1' if the direction and polarity were clearly determined (mostly from Group B); 'Quality 2' if the polarity is clearly determined but not the direction such as when using anchored line fits (mostly Groups A and C); and 'Quality 3' if neither direction nor polarity is clearly determined although a direction can be calculated (mostly Groups A and C).

Most ChRM directions from the Bashibulake Formation (Group A) clearly depart from the rest of the directions from the overlying formations. They are in a normal polarity orientation before tilt-correction strongly suggesting post-folding remagnetization. This is similar to paleomagnetic results obtained from the marine red sediments of the Wulagen Formation obtained in the west central Tarim Basin. Together these results suggest that marine sediments from the Tarim Basin have similar magnetic properties yielding remagnetizations. Caution should be used when interpreting paleomagnetic result from these rocks to infer magnetostratigraphic ages or tectonic rotation (see Bosboom et al., 2014a,b,c). These directions were discarded by applying the following procedure.

In order to systematically filter out unreliable directions, Virtual Geomagnetic Pole (VGP) directions were calculated from the ChRM directions and VGP directions that were more than 45° from the mean VGP were iteratively discarded (see Dupont-Nivet and Krijgsman, 2012). This was done separately for normal and reversed polarity directions. After bedding tilt correction, the remaining directions separate into two antipodal clusters of normal and reversed polarities.

To assess the primary nature of the selected ChRM directions the reversal and fold tests were applied to this dataset (Tauxe, 1998). The fold test is clearly positive with clustering of directions at maximum unfolding indicating a pre-folding acquisition of the ChRM (Fig. 5). The reversal test, however, is not positive at the 95% confidence level although the directions are close to antipodal. This probably results from the incomplete separation of components of samples from Group C and even possibly the presence of an unidentified overlapping normal component in some sample of Group B with an apparent linear trajectory towards the origin. The absence of a positive reversal test, however, does not affect the reliability of the magnetostratigraphy based on the correct determination of polarities rather than directions (see Dupont-Nivet and Krijgsman, 2012).

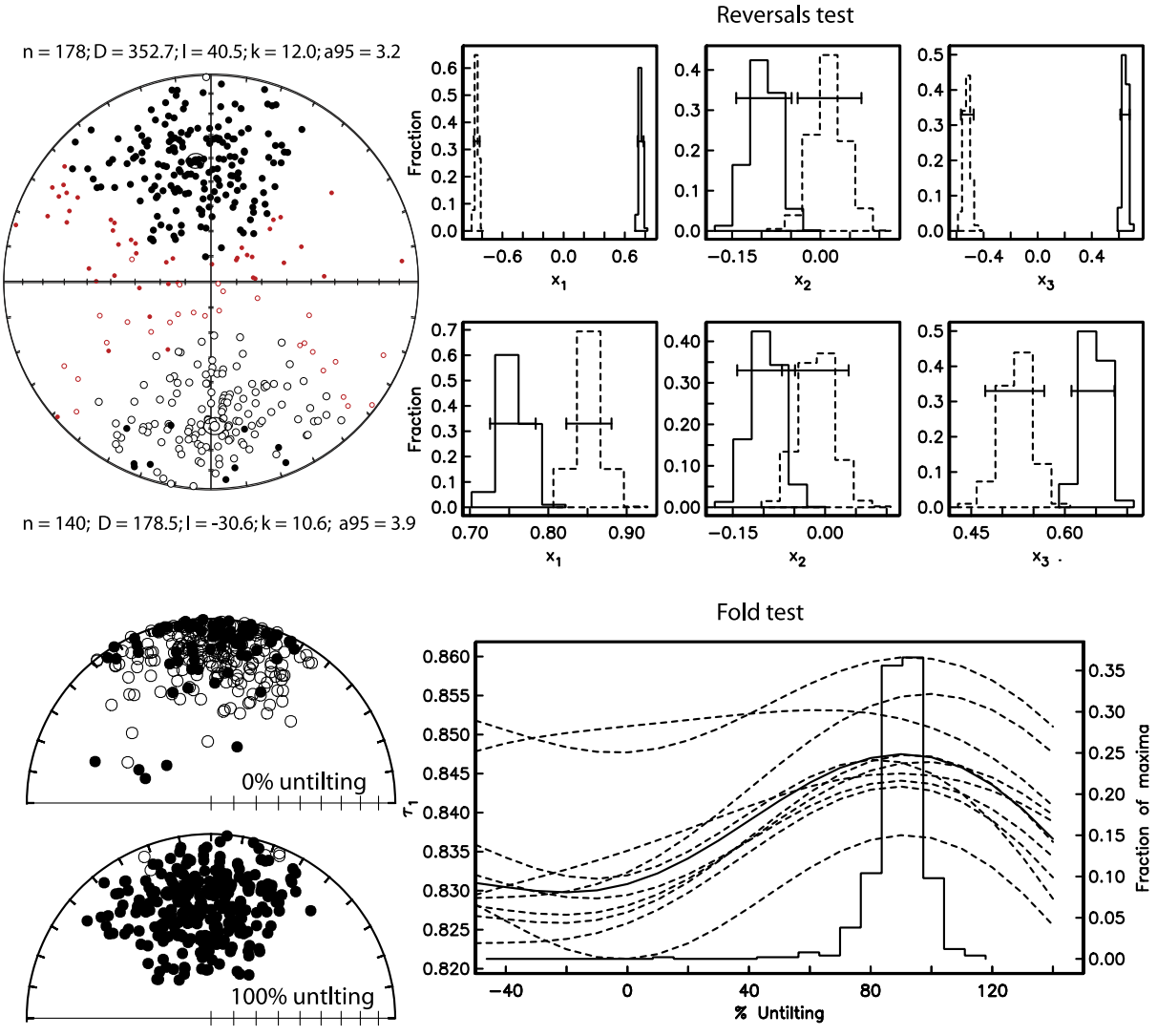

Fig. 5. ChRM directions, reversals and fold test. Full (open) symbols are projections on the lower (upper) hemisphere.

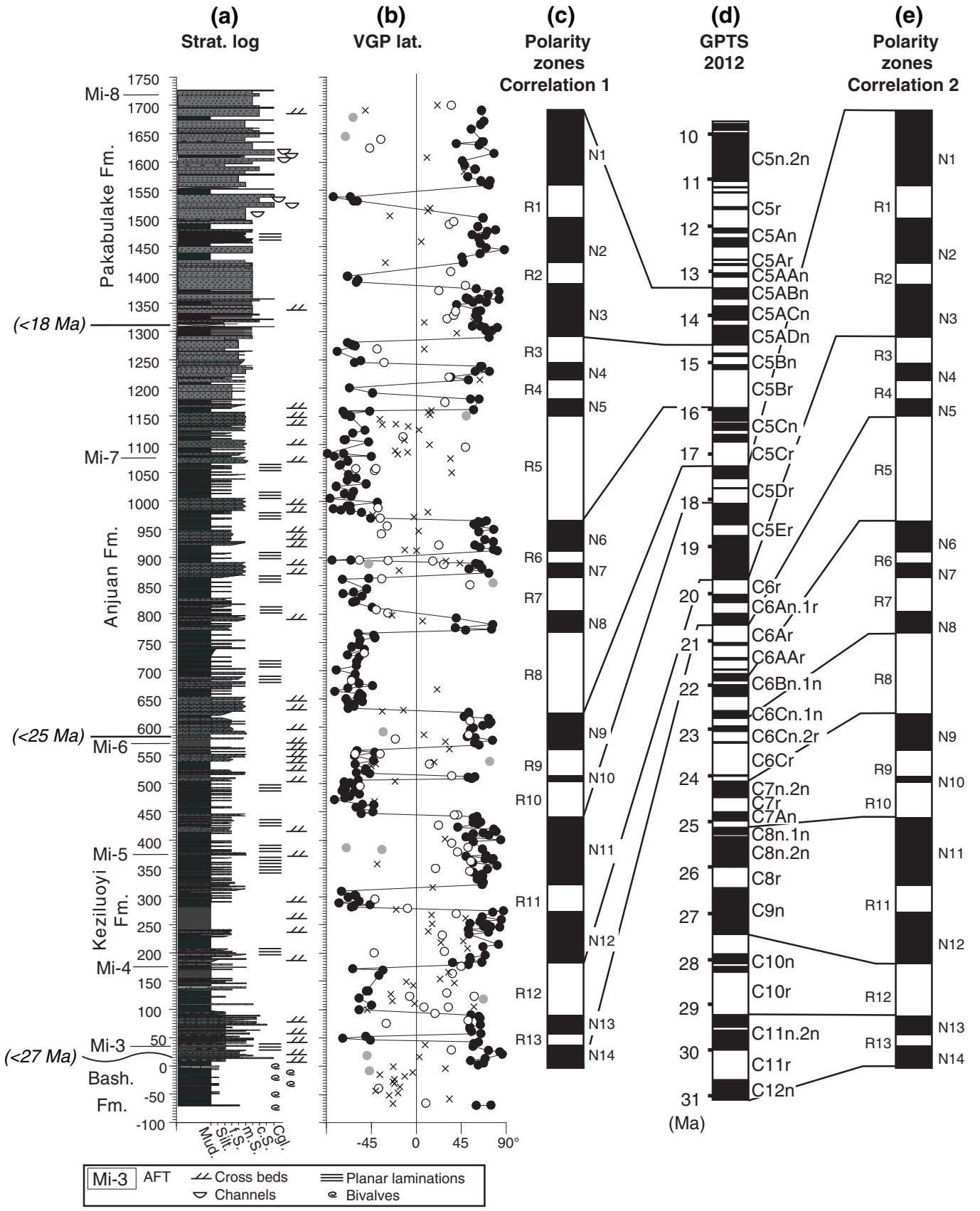

Fig. 6. Magnetostratigraphy of the Mine section. (a) Stratigraphic description of the measured section in meters (m). (b) VGP latitude represented by full circles (reliable 'Quality 1 directions' used to construct the magnetic polarity zones), open circles (outlying 'Quality 2' directions that have been discarded by applying an iterative 45° cutoff) and crosses (unreliable 'Quality 3' directions that have been discarded, see text). Gray dots are isolated polarity directions that have been systematically discarded. (c) Corresponding magnetic polarity zones with preferred correlation 1 and (e) alternative correlation 2 (see text). (d) GPTS 2012: geomagnetic polarity time scale (Gradstein et al., 2012). Maximum depositional age constraints from apatite fission track analyses (Yang et al., 2014).

6.3. Magnetostratigraphic correlation

Polarity zones were defined by at least two consecutive levels yielding accepted VGP latitudes with the same polarity (Fig. 6). This resulted in the definition of a total of 14 normal and 13 reversed polarity intervals recorded in this section, marked as N1–N14 and R1–R13 from top to bottom, respectively (Fig. 6).

Correlation to the geomagnetic polarity time scale (GPTS 2012) of Gradstein et al. (2012) was initially guided by age constraints arising from biostratigraphic constraints of the underlying marine deposits of the Bashibulake Formation dated late Bartonian–early Priabonian (38.5–35.5 Ma). However, these sediments are separated from the overlying Keziluoyi Formation at the base of our section by a slight angular unconformity of unknown duration. Additional constraints are provided by the youngest population of detrital AFT ages presented above. For the Keziluoyi Formation the younger clusters of AFT ages range from ca. 27 Ma at the base (35 meter-level) to ca. 25 Ma at the top (570 meter-level). Additional constraints are provided for the upper part in the Anjuan Formation at the 1075 meter-level by the youngest detrital AFT ages around 18 Ma (18.2 ± 7.8 and 18.5 ± 9.8 Ma). These clusters of detrital AFT ages actually represent exhumation ages that are therefore older than the depositional age depending on the lag time (Bernet and Spiegel, 2004). These considerations provide a relatively broad timeframe on which we explored for possible magnetostratigraphic correlations based on the pattern of observed polarity zones.

As a starting point, we consider the longest and conspicuous reversed polarity zone R5 that includes the AFT ages ca. 18 Ma. Long reversed chrons around that time that may be correlated with R5 are C5r (ca. 11.5 Ma), C5Br (ca. 15.5 Ma), C5Cr (ca. 17 Ma), C6Ar together with C6AAr (ca. 21 Ma, assuming that short normal chrons within have been missed) or C6Cr (ca. 23.5 Ma). Several of these options can be immediately rejected given the rest of the recorded polarity pattern observed above and below R5. Above R5, two short normal zones precede three very large normal zones separated by short reversed zones. This enables us to exclude correlating N5 with C5Cr because this pattern does not correspond to the very long C5n above C5r. It also excludes correlating N5 with C5Cr because the long reversed C5Br would not be found in the observed pattern above N5. Correlating N5 with C6Cr is not excluded by the observed pattern above N5 but very unlikely given the pattern below N5 with three short normal zones separated by short reversed zones and underlain by another long reversed zone R8. This pattern below N5 cannot be reconciled by the dominantly normal chron pattern below C6Cr such that this correlation is rejected. We now consider the two remaining possible correlations, N5 with C5Br (correlation 1) or N5 with C6Ar and C6AAr (correlation 2) illustrated on Figs. 6 and 7. Both yield realistic rates ranging from about 5 to 50 cm/kyr without major fluctuations although more fluctuations are observed for correlation 2. In both correlations, average rates increase upsection in agreement with the coarsening upward lithologies. An abrupt increase in rates is observed within R11 (C9n ca. 28–27 Ma) and within N11 (C5Er ca. 19–17 Ma) respectively for correlations 1 and 2. For correlation 1, the increase corresponds to the apparition and increase of siltstone and sandstone beds while there is no lithologic change associated with the rate increase for correlation 2 within a dominantly mudstone interval.

Correlation 2 is found less likely because it requires several normal chrons to have been missed throughout the correlation. In particular, within R5, R7 and R8 while these intervals are well defined by high-resolution sampling yielding reliable ChRMs, it is also less favored because it would imply a 21 Ma depositional age at the 1075 meter-level that yielded detrital AFT ages ca. 18 Ma. Correlation 1 is found more likely as it provides a realistic correlation for each of the observed polarity zones without missing any chrons. The pattern fit is optimal with the exception of R7 that is slightly too thick. This correlation is also favored by the record of detrital AFT ages. Correlation 1 yields a depositional age ca. 15.5 Ma for the 1075 meter-level that is realistically younger than the AFT ca. 18 Ma age cluster obtained at this level.

In summary, based on the most likely correlation to the GPTS (Gradstein et al., 2012), the Keziluoyi Formation was deposited at the Mine section between 20.6 Ma and 17.5 Ma. The Anjuan Formation was deposited from 17.5 to 14.6 Ma, and the overlying Pakabulake Formation initiated with the first conglomerate at around 14.6 Ma. Based on age constraints of correlation 1, sediment accumulation rates can be directly determined using thicknesses between identified reversals of known age throughout the section (Table 2). A mark increase in accumulation rates ca. 19–18 Ma (within polarity zone R11) is observed

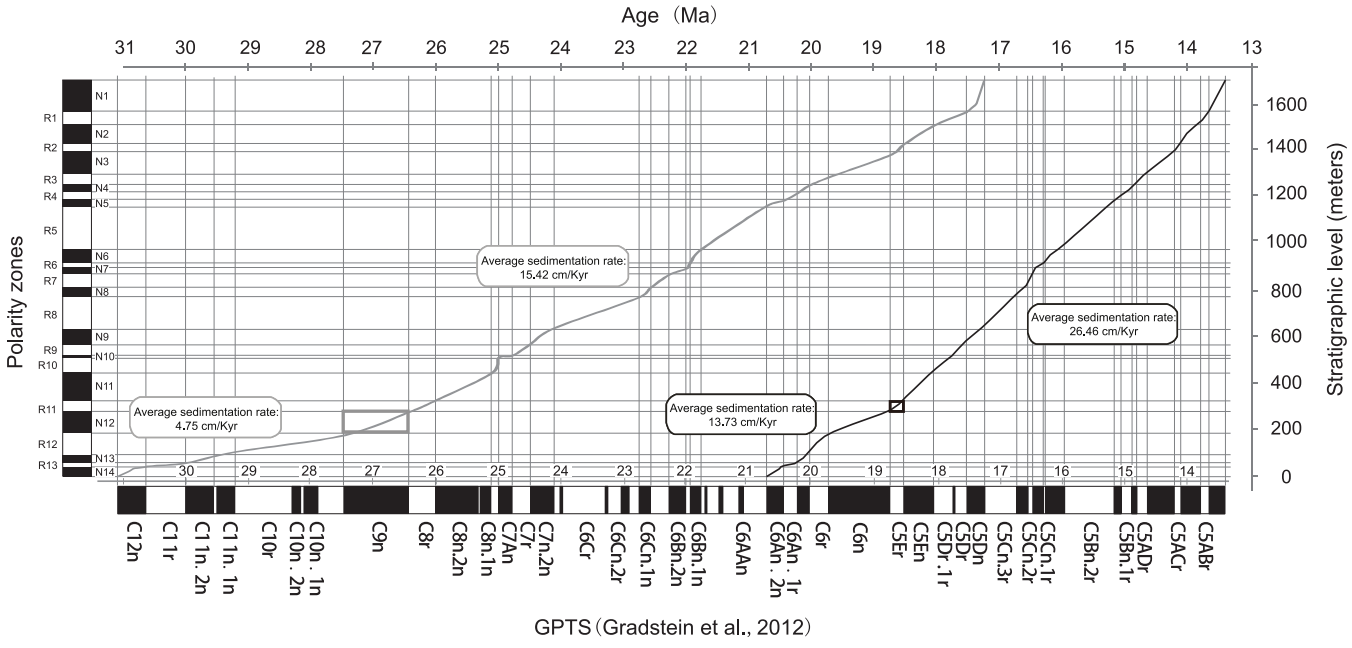

Fig. 7. Correlation of the polarity zones recognized in the Mine section to the GPTS 2012 (Gradstein et al., 2012). The preferred (alternative) correlation is represented by the thick black (gray) line with corresponding accumulation rates and identified increase in accumulation rates indicated by black (gray) boxes.

Table 2
Sedimentation accumulation rates.

Level (m)	Polarity zones	Preferred correlation				Rejected correlation			
		Chron	Age (Ma)	Rate (cm/kyr)	Av. rate (cm/kyr)	Chron	Age (Ma)	Rate (cm/kyr)	Av. rate (cm/kyr)
6.00	Base N14	Top C6Ar	20.709	13.80	13.73	Top C12r	31.034	8.41	4.75
43.25	R13	Base C6An.1r	20.439	6.37		Base C11r	30.591	2.32	
57.65		Top C6An.1r	20.213	27.25		Top C11r	29.970	5.99	
104.8	R12	Base C6r	20.040	22.59		Base C10r	29.183	4.12	
176.65		Top C6r	19.722	10.11		Top C9r	27.439	9.67	
275.15	R11	Base C5Er	18.748	22.41		Base C8r	26.420	11.59	15.42
325.35		Top C5Er	18.524	24.91	26.46	Top C8r	25.987	13.13	
441.95	R10	Base C5Dr.1r	18.056	21.17		Base C7Ar	25.099	58.17	
508.85		Top C5Dr.1r	17.740	38.70		Top C7Ar	24.984	3.99	
517.75	R9	Base C5Dr	17.717	27.45		Base C7r	24.761	17.60	
568.25		Top C5Dr	17.533	21.98		Top C7r	24.474	17.95	
633.75	R8	Base C5Cn.3r	17.235	25.72		Base C7n.1r	24.109	9.76	
765.95		Top C5Cn.3r	16.721	23.65		Top C6Cn.1r	22.754	22.16	
808.05	R7	Base C5Cn.2r	16.543	78.17		Base C6Br	22.564	18.75	
863.55		Top C5Cn.2r	16.472	15.80		Top C6Br	22.268	9.67	
890.25	R6	Base C5Cn.1r	16.303	62.00		Base C6Bn.1r	21.992	38.75	
911.95		Top C5Cn.1r	16.268	19.80		Top C6Bn.1r	21.936	34.44	
970.15	R5	Base C5Bn.2r	15.974	23.21		Base C6AAr.3r	21.767	17.85	
1159.05		Top C5Bn.2r	15.160	17.19		Top C6Ar	20.709	8.15	
1181.05	R4	Base C5Bn.1r	15.032	20.62		Base C6An.1r	20.439	14.78	
1214.45		Top C5Bn.1r	14.870	32.00		Top C6An.1r	20.213	17.57	
1244.85	R3	Base C5ADr	14.775	21.69		Base C6r	20.040	11.32	
1280.85		Top C5ADr	14.609	21.21		Top C6r	19.722	9.71	
1375.45	R2	Base C5ACr	14.163	50.11		Base C5Er	18.748	20.80	
1422.05		Top C5ACr	14.070	23.87		Top C5Er	18.524	16.88	
1501.05	R1	Base C5ABr	13.739	44.58		Base C5Dr.1r	18.056	11.17	
1559.45		Top C5ABr	13.608	53.71		Top C5Dr	17.533	44.16	
1691.05	Top N1	Base C5AAr	13.363	–		Base C5Cn.3r	17.235	–	

Notes: Level — stratigraphic level from the studied section; Age — age of correlated chron based on GPTS 2012 (Gradstein et al., 2012); Rate — calculated sediment accumulation rate; Av. rate — average rate for longer intervals.

between the lower part (average 13.73 cm/kyr) and the upper part (average 26.46 cm/kyr) of the record (Fig. 7). We discuss below the potential tectonic significances of these results.

7. Discussion

Our results reveal that the Keziluoyi strata, previously assigned to the Oligocene, are in fact Miocene. At the studied section, the onset of continental deposits at 20.8 Ma overlies directly the last marine deposits of the marine Bashibulake Formation recently dated using biostratigraphy to late Eocene age between the late Bartonian and early Priabonian (38.5–35.5 Ma; Bosboom et al., 2014a). This implies a major Oligocene hiatus in the southwestern Tian Shan foreland basin. This very long discontinuity may reflect a major erosional event and/or the prolonged absence of sediment accumulation.

The latter is supported by several observations. At the Mine section this major hiatus recognized between the Bashibulake and overlying Keziluoyi Formations occurs at the 15 meter level and is expressed by a fine gravel layer of ~0.5 m thickness. The angle of the unconformity is less that a few degrees and discernible only on extensive outcrops over several hundreds of meters in length (Fig. 3). The contact between these Formations is reported as a parallel disconformity upon Cretaceous to Eocene strata in other sections of the Wuqia area and further east in the Kashi foreland (Ulugqat; Jin et al., 2003; Heermance et al., 2007).

Also suggesting that the hiatus does not stem from a major erosional event, is that the Bashibulake Formation represents the youngest marine deposits regionally reported below the Keziluoyi Formation (see Bosboom et al., 2014a, and references therein). Furthermore, at the Mine section, the complete stratigraphy of the five members of the Bashibulake Formation found below the hiatus represents the maximum thickness for this formation reported in the region (Jin et al., 2003). We thus infer that little erosion affected the Bashibulake Formation preserved at the Mine section below the hiatus. This non-erosive Oligocene hiatus is, according to existing magnetostratigraphic records of continental deposits, widespread in the southwestern Tian Shan (Kashi foreland; Heermance et al., 2007, 2008) thus suggesting little to no deformation between deposition of Eocene strata and the initiation of Neogene southwestern Tian Shan uplift. This is also in excellent agreement with the thermochronologic data showing exhumation ages not older than ca. 25 Ma as expressed by detrital apatite fission track data from the studied Mine section (see above and Yang et al., 2013) but also throughout the southwestern Tian Shan ranges (Sobel et al., 2006).

In southwestern Tarim (Yecheng sub-basin, Fig. 1), this large hiatus is not present in the recently dated marine to continental transition (Bosboom et al., 2014b). There, the marine deposits ending with the Wulagen Formation are conformably overlain by the ca. 41 Ma continental deposits of the Keziluoyi Formation. Given the significantly different ages for the Keziluoyi deposits in the Yecheng sub-basin and those studied here, it may seem awkward to give them identical names. However, we prefer preserving the original Keziluoyi denomination to avoid confusion. In fact, the Keziluoyi Formation in southwestern Tarim is time equivalent to the marine Bashibulake Formation found in northwestern Tarim (but not present in southwestern Tarim) and continuously deposited through the Oligocene except for a gap including the Eocene–Oligocene transition as constrained with magnetostratigraphy (see Bosboom et al., 2014b). Thick continuous deposition through the Oligocene in southwestern Tarim and the coeval lack of accumulation in Northwestern Tarim along the southern Tian Shan are consistent with Tarim isopach maps (Wei et al., 2014; Yang and Liu, 2002). Our results thus support a simple model for the evolution of the basin with subsidence starting in the southwest in response to Eocene to Oligocene Kunlun Shan northward thrusting (e.g. Jolivet et al., 2001) while the southwestern Tian Shan foreland remained mostly inactive until the early Miocene onset of subsidence and accumulation associated with Tian Shan exhumation (e.g. De Grave et al., 2012; Dumitru et al., 2001; Hendrix et al., 1994; Sobel et al., 2006; Wang et al., 2009) (Fig. 8).

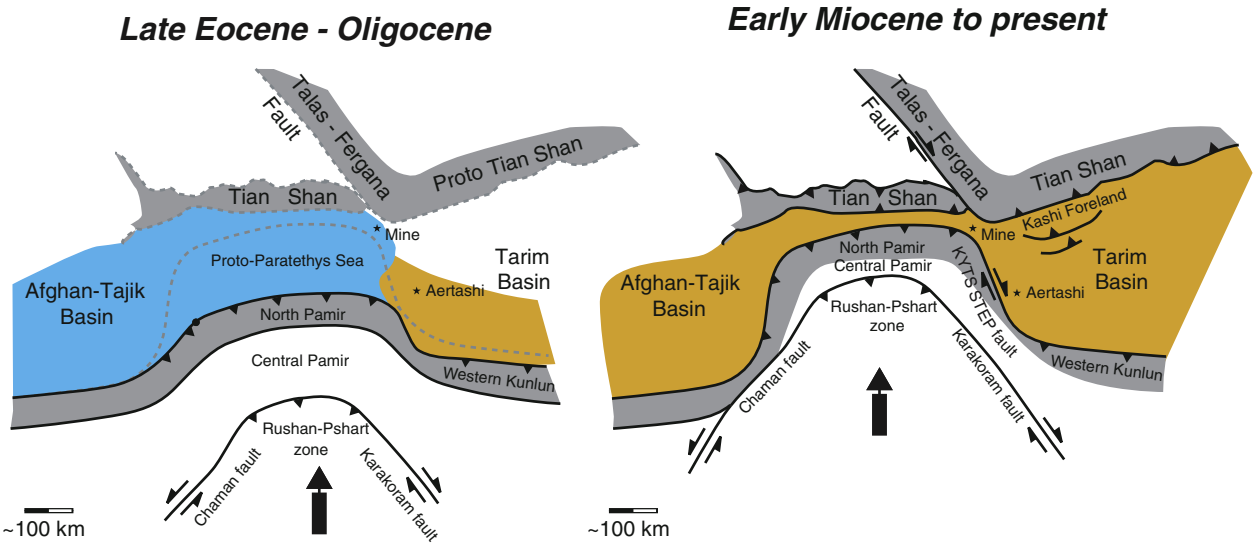

Fig. 8. Proposed tectonic and paleogeographic evolution of the Pamir salient and the southwestern Tian Shan (modified after Cowgill, 2010), based upon results of this study and previous studies of the proto-Paratethys Sea and southwestern Tian Shan (Bosboom et al., 2014a, b; Coutand et al., 2002; Lan and Wei, 1995; Tang et al., 1989). The paleogeographic evolution is shown with the approximate extent of the sea shaded in blue and approximate extent of basin accumulation shaded in yellow for the Late Eocene–Oligocene (a) and Early Miocene to present (b).

After the major hiatus at the Mine section, overlying continental sediments of the basal Keziluoyi Formation start being deposited at 20.8 Ma. These sediments yield a young cluster of AFT detrital ages ca. 27–25 Ma and a notable increased diversity of U/Pb ages indicating recycling of material from the Paleozoic and Mesozoic southwest Tian Shan piedmont (Yang et al., 2014). This suggests that the deposition of the Keziluoyi Formation can be associated with the early Miocene south Tian Shan exhumation (De Grave et al., 2012; Dumitru et al., 2001; Sobel et al., 2006; Wang et al., 2009). Our results fit well within the regional model of southward propagation of deformation of the Kashi foreland basin constrained by magnetostratigraphy and thermochronology (Heermance et al., 2007, 2008; Sobel et al., 2006). These indicate an onset of exhumation at the Oligocene–Miocene boundary (~24 Ma) along thrust sheets (the Maidan and Muziduke thrusts, which bound the southern side of the Kokshaal range) that are located on the other side of the Talas Fergana fault to the east. This suggests that the timing of the onset of south Tian Shan exhumation was similar on either side of the Talas Fergana fault.

Further up in the Mine section, we report a significant increase in sediment accumulation at ~18.5 Ma (Fig. 7 and Table 2), coeval with a lithologic transition from dominantly red-brown mudstones to more fluvial dark mudstones and gray-green sandstones. This age compares well with results from the detrital apatite fission track dating from the nearby Ulugqat section (Yang et al., 2014). There, two sandstone samples (UC01 from Middle Jurassic strata and UC02 from Early Cretaceous strata) yield central fission track ages of 18.5 ± 5.2 and 16.6 ± 2.8 Ma, respectively. These two samples are interpreted to be totally reset with the central AFT ages representing the age of subsequent exhumation. This suggests that thrust sheets north of the Mine section propagated southwards at this time inducing the increased accumulation rates and the cluster of ca. 18 Ma detrital AFT ages in associated sediments of the Mine section. Regionally, this age corresponds well with the 18.9 ± 3.3 Ma southward propagation of deformation into the Kashi foreland basin (the Kashi basin-bounding thrust, Sobel et al., 2006) with associated southward propagating increased accumulation rates and conglomeratic deposition (Xiyu Formation) into the Kashi basin from 15.5 Ma onwards (Heermance et al., 2007). However, the appearance of the conglomeratic Xiyu Formation appears to be delayed at the Mine section. There the conglomerates occur stratigraphically ca. 1400 m above the top of the measured section. Assuming constant average accumulation rates (26 cm/kyr, Table 2) from the top of the section at 13.4 Ma, this allows a rough estimate of 8.0 Ma for the appearance of the Xiyu conglomerates. This is significantly younger than the 15.5 Ma Xiyu appearance reported from the equivalent portion of the Kashi foreland east of the Talas Fergana Fault (TFF). This suggests that at 15.5 Ma, thrusting into the foreland basin had propagated further southward east of the TFF compared to west. This suggests that the TFF was already active, affecting Tian Shan deformation and possibly responding to far field effect of the Pamir indentation as discussed below in view of the regional tectonic setting.

Finally, our results are concordant in time and space with recently proposed models for the tectonic evolution of the Pamir salient (Bosboom et al., 2014c; Cowgill, 2010; Sobel et al., 2013). During the Early Eocene–Late Oligocene, deformation was far to the south of the south Tian Shan as the Pamir began to indent into Tarim with exhumation along the Kunlun Shan. Exhumation started in the Tian Shan near the Oligo-Miocene boundary but propagated southwards ca. 20–18 Ma.This time corresponds to the initiation of the Kashgar–Yecheng Transfer System (KYTS), the main 300 km dextral slip shear zone separating Tarim from the Eastern Pamir (Cao et al., 2013; Cowgill, 2010; Sobel and Dumitru, 1997; Sobel et al., 2006, 2011) (Fig. 8). We thus propose that already ca. 20–18 Ma, far-field effects of this Pamir indentation transferred deformation northward from the India–Asia collision zone, across the Tarim Basin and into the Southwestern Tian Shan, enhancing thrusting and exhumation and possibly reactivating the Talas Fergana Fault.

8. Conclusions

We show using magnetostratigraphy that the onset of continental deposition recorded in the Keziluoyi Formation – previously attributed to the Oligocene – actually started in the early Miocene in the southwestern Tian Shan. This reveals the existence of a major hiatus between these continental deposits and the underlying marine successions recently dated as late Eocene (38.5–35.5 Ma; Bosboom et al., 2014a). Compared with the coeval thick Oligocene foreland deposition in southwestern Tarim, this hiatus shows that the Oligocene was relatively quiet along the southern Tian Shan piedmont. This support a simple model for the Tarim Basin evolution with subsidence starting in the southwest in response to Eocene to Oligocene Kunlun Shan northward

thrusting followed only much later by the early Miocene onset of subsidence associated with Tian Shan exhumation together with the reactivation of the Talas Fergana Fault. This time also corresponds to the activation of a major strike-slip system along the eastern Pamir indentation suggesting that far-field effects of the India–Asia collision started to transfer to the Tian Shan across Tarim.

Our results show that the India–Asia deformation had not propagated to the Tian Shan before the early Miocene, thus raising the question: why did it not propagate previously? A simple explanation is that progressive northward propagation of deformation did not reach the Tian Shan until the early Miocene (e.g. Tapponnier et al., 2001). Alternatively, it is possible that the collision itself changed drastically in the early Miocene to be able to propagate deformation much further into Asia. This may result, as previously proposed, from a change from soft to hard collision related to various stages of slab break off (e.g. Chemenda et al., 2000) and/or to a two stage collision with the actual continental collision occurring only in the early Miocene (e.g. Van Hinsbergen et al., 2012).

Acknowledgments

This work was supported by the Science Foundation of China University of Petroleum, Beijing (No. 2462014YJRC023), by the Foundation of State Key Laboratory of Petroleum Resources and Prospecting, China University of Petroleum, Beijing (No. PRP/indep-4-1406), by the Cai Yuanpei program from the French Ministry of Foreign Affairs and Ministry of Higher Education and Research and the Ministry of Education of the People's Republic of China (DOSSIER N°30137), by a VIDI grant from the Netherlands Organisation for Scientific Research (NWO), by the Marie Curie Career Integration Grant (294282). We acknowledge the constructive comments from three reviewers and we are very grateful to Annick Chauvin, Pierrick Roperch, Philippe Cullerier, Philippe Dufresne and Lucie Garnier for their great help in the Paleomagnetic laboratory.

Appendix A. Supplementary data

Supplementary data to this article can be found online at http://dx.doi.org/10.1016/j.tecto.2015.01.003.

References

Amidon, W.H., Hynek, S.A., 2010. Exhumation history of the north central Pamir. Tectonics 29. http://dx.doi.org/10.1029/2009TC002589 (TC5017).

Avouac, J.P., Tapponnier, P., Bai, M.H., You, H., Wang, G., 1993. Active thrusting and folding along the northern Tian Shan and late Cenozoic rotation of the Tarim relative to Dzungaria and Kazakhstan. J. Geophys. Res. 98, 6755–6804.

Bernet, M., Spiegel, C., 2004. Introduction: detrital thermochronology. In: Bernet, M., Spiegel, C. (Eds.), Detrital Thermochronology — Provenance Analysis, Exhumation and Landscape Evolution of Mountain Belts. Geological Society of America Special Publication 378, pp. 1–6.

Bershaw, J., Garzione, C.N., Schoenbohm, L., Gehrels, G., Li, T., 2012. Cenozoic evolution of the Pamir plateau based on stratigraphy, zircon provenance, and stable isotopes of foreland basin sediments at Oytag (Wuyitake) in the Tarim Basin (west China). J. Asian Earth Sci. 44 (30), 136–148.

BGMRXUAR (Bureau of Geology and Mineral Resources of Xinjiang Uygur Autonomous Region), 1993. Regional Geology of Xinjiang Uygur Autonomous Region. Geological Publishing House, Beijing (841 pp. (in Chinese)).

Bosboom, R.E., Dupont-Nivet, G., Houben, A.J.P., Brinkhuis, H., Villa, G., Mandic, O., Stoica, M., Zachariasse, W.J., Guo, Z.J., Li, C.X., Krijsman, W., 2011. Late Eocene sea retreat from the Tarim Basin (west China) and concomitant Asian paleoenvironmental change. Palaeogeogr. Palaeoclimatol. Palaeoecol. 299, 385–398.

Bosboom, R.E., Dupont-Nivet, G., Grothe, A., Brinkhuis, H., Villa, G., Mandic, O., Stoica, M., Kouwenhoven, T., Huang, W., Guo, Z.J., 2014a. Paleogeography of the late Eocene stepwise sea retreat from the Tarim Basin (west China). Palaeogeogr. Palaeoclimatol. Palaeoecol. 403, 101–118.

Bosboom, R., Dupont-Nivet, G., Grothe, A., Brinkhuis, H., Villa, G., Mandic, O., Stoica, M., Huang, W., Yang, W., Guo, Z., Krijgsman, W., 2014b. Linking Tarim Basin sea retreat (west China) and Asian aridification in the late Eocene. Basin Res. 26 (5), 621–640.

Bosboom, R.E., Dupont-Nivet, G., Huang, W., Yang, W., Guo, Z.J., 2014c. Oligocene clockwise rotations along the eastern Pamir: tectonic and paleogeographic implications. Tectonics 33 (2), 53–66.

Bullen, M.E., Burbank, D.W., Garver, J.I., Abdrakhmatov, K.Y., 2001. Late Cenozoic tectonic evolution of the northwestern Tien Shan: new age estimates for the initiation of mountain building. Geol. Soc. Am. Bull. 113 (12), 1544–1559.

Bullen, M.E., Burbank, D.W., Garver, J.I., 2003. Building the northern Tien Shan: integrated thermal, structural, and topographic constraints. J. Geol. 111, 149–165.

Burchfiel, B.C., Royden, L.H., 1991. Tectonics of Asia 50 years after the death of Emile Argand. Eclogae Geol. Helv. 84, 599–629.

Burchfiel, B.C., Brown, E.T., Deng, Q.D., Feng, X.Y., Li, J., Monlar, P., Shi, J.B., Wu, Z.M., You, H.C., 1999. Crustal shortening on the margins of the Tien Shan, Xinjiang, China. Int. Geol. Rev. 41, 665–700.

Burtman, V.S., 2000. Cenozoic crustal shortening between the Pamir and Tien Shan and a reconstruction of the Pamir–Tien Shan transition zone for the Cretaceous and Palaeogene. Tectonophysics 319, 69–92.

Burtman, V.S., Molnar, P., 1993. Geological and geophysical evidence for deep subduction of continental crust beneath the Pamir. Geol. Soc. Am. Spec. Pap. 281.

Buslov, M.M., De Grave, J., Bataleva, E.A.V., 2004. Cenozoic tectonics and geodynamic evolution of the Tien Shan mountain belt. Himal. J. Sci. 2, 106–107.

Buslov, M.M., De Grave, J., Bataleva, E.A.V., Batalev, V.Y., 2007. Cenozoic tectonic and geodynamic evolution of the Kyrgyz Tien Shan Mountains: a review of geological, thermochronological and geophysical data. J. Asian Earth Sci. 29, 205–214.

Cao, K., Wang, G.C., Liu, C., Meng, Y.N., 2009. Thermochronological evidence of the Cenozoic differential uplift process of the West Kunlun and its adjacent area. Earth Sci. J. China Univ. Geosci. 34 (6), 895–906 (in Chinese with English abstract).

Cao, K., Wang, G.C., Beek, P.V.D., Bernet, M., Zhang, K.X., 2013. Cenozoic thermo-tectonic evolution of the northeastern Pamir revealed by zircon and apatite fission-track thermochronology. Tectonophysics 589, 17–32.

Charreau, J., Chen, Y., Gilder, S., Dominguez, S., Avouac, J.-P., Sen, S., Sun, D., Li, Y., Wang, W.M., 2005. Magnetostratigraphy and rock magnetism of the Neogene Kuitun He section (Northwest China): implications for Late Cenozoic uplift of the Tianshan Mountains. Earth Planet. Sci. Lett. 230, 177–192.

Charreau, J., Chen, Y., Gilder, S., Barrier, L., Dominguez, S., Augier, R., Sen, S., Avouac, J.P., Gallaud, A., Graveleau, F., WANG, Q., 2009. Neogene uplift of the Tian Shan Mountains observed in the magnetic record of the Jingou River section (northwest China). Tectonics 28 (2). http://dx.doi.org/10.1029/2007TC002137.

Chemenda, A.I., Burg, J.-P., Mattauer, M., 2000. Evolution model of the Himalaya–Tibet system: geopoem based on new modeling, geological and geophysical data. Earth Planet. Sci. Lett. 174, 397–409.

Chen, J., Burbank, D.W., Scharer, K.M., Sobel, E., Yin, J.H., Rubin, C., Zhao, R.B., 2002. Magnetochronology of the Upper Cenozoic strata in the Southwestern Chinese Tian Shan: rates of Pleistocene folding and thrusting. Earth Planet. Sci. Lett. 195, 113–130.

Coutand, I., Strecker, M.R., Arrowsmith, J.R., Hilley, G., Thiede, R.C., Korjenkov, A., Omuraliev, M., 2002. Late Cenozoic tectonic development of the intramontane Alai Valley, (Pamie–Tien Shan region, central Asia): an example of intracontinental deformation due to the Indo-Eurasia collision. Tectonics 21 (6), 1053. http://dx.doi.org/10.1029/2002TC001358.

Cowgill, E., 2010. Cenozoic right-slip faulting along the eastern margin of the Pamir salient, northwestern China. Geol. Soc. Am. Bull. 122 (1–2), 145–161.

Cui, J.W., Guo, X.P., Ding, X.Z., Li, P.W., Zhang, X.W., 2006. Mesozoic–Cenozoic deformation structures and their dynamics in the basin-range junction belt of the west Kunlun–Tarim basin. Front. Earth Sci. Chin. 13 (4), 103–118 (in Chinese with English abstract).

De Grave, J., Glorie, S., Ryabinin, A., Zhimulev, F., Buslov, M.M., Lzmer, A., Elburg, M., Vanhaecke, F., Van den haute, P., 2012. Late Paleozoic and Meso-Cenozoic tectonic evolution of the southern Kyrgyz Tien Shan: constraints from multi-method thermochronology in the Trans-Alai, Turkestan-Alai segment and the southeastern Fergana Basin. J. Asian Earth Sci. 44, 149–168.

Dumitru, T.A., Zhou, D., Chang, E.Z., Graham, S.A., 2001. Uplift, exhumation, and deformation in the Chinese Tian Shan. In: Hendrix, M.S., Davis, G.A. (Eds.), Paleozoic and Mesozoic Tectonic Evolution of Central Asia: From Continental Assembly to Intracontinental Deformation. Geological Society of America Memoirs 194, pp. 71–99.

Dupont-Nivet, G., Krijgsman, W., 2012. Magnetostratigraphic methods and applications. In: Busby, C., Azor, A. (Eds.), Recent Advances in Tectonics of Sedimentary Basins. Wiley-Blackwell, pp. 80–94.

Dzhalilov, M.R., Alekseev, M.N., Andreev, Y.N., Salibaev, G.K., 1982. Mesozoic and Cenozoic deposits of the northern part of the Afghano-Tajik Basin. Miner. Resour. Dev. Ser. 131.

Fang, S.H., Guo, Z.J., Song, Y., Wu, C.D., Zhang, Z.C., Wang, M.N., Fan, R.D., 2005. Sedimentary facies evolution and basin pattern of the Jurassic in southern margin area of Junggar Basin. J. Palaeogeogr. 7 (3), 347–356 (in Chinese with English abstract).

Fang, S.H., Guo, Z.J., Wu, C.D., Zhang, Z.C., Wang, M.N., Yuan, Q.D., 2006. Jurassic clastic composition in the southern Junggar Basin, Northwest China: implications for basin-range pattern and tectonic attributes. Acta Geol. Sin. 80 (2), 196–209 (in Chinese with English abstract).

Gao, Z.J., Chen, K.Q., Wei, J.Y., 2000. The Lithostratigraphic Dictionary of China. The Press of Geological University, Beijing (627 pp. (in Chinese)).

Garzione, C., Ikari, M.J., Basu, A.R., 2005. Source of Oligocene to Pliocene sedimentary rocks in the Linxia basin in northeastern Tibet from Nd isotopes: implications for tectonic forcing of climate. Geol. Soc. Am. Bull. 117 (9), 1156–1166.

Gradstein, F.M., Ogg, J.G., Schmitz, M., Ogg, G., 2012. The Geological Time Scale 2012. Elsevier.

Graham, S.A., Page Chamberlain, C., Yue, Y.J., Ritts, B., Hanson, A.D., Horton, T.W., Waldbauer, J.R., Poage, M.A., Feng, X., 2005. Stable isotope records of Cenozoic climate and topography, Tibetan plateau and Tarim basin. Am. J. Sci. 305 (2), 101–118.

Hao, Y.S., Guan, S., Ye, L., Huang, Y., Zhou, Y., Guan, S., 2002. Neogene stratigraphy and paleogeography in the western Tarim basin. Acta Geol. Sin. 76 (3), 289–298 (in Chinese with English abstract).

Heermance, R.V., Chen, J., Burbank, D.W., Wang, C.S., 2007. Chronology and tectonic controls of Late Tertiary deposition in the southwestern Tian Shan foreland, NW China. Basin Res. 19, 599–632. http://dx.doi.org/10.1111/j.1365-2117.2007.00339.x.

Heermance, R.V., Chen, J., Burbank, D.W., Miao, J., 2008. Temporal constraints and pulsed Late Cenozoic deformation during the structural disruption of the active Kashi foreland, northwest China. Tectonics 27. http://dx.doi.org/10.1029/2007TC002226.

Hendrix, M.S., 2000. Evolution of Mesozoic sandstone compositions, southern Junggar, northern Tarim, and western Turpan basins, Northwest China: a detrital record of the ancestral Tian Shan. J. Sediment. Res. 70 (3), 520–532.

Hendrix, M.S., Dumitru, T.A., Graham, S.A., 1994. Late Oligocene–early Miocene unroofing in the Chinese Tian Shan: an early effect of the India–Asia collision. Geology 22, 487–490.

Huang, B.C., Piper, J.-D.A., Peng, S., Liu, T., Li, Z., Wang, Q., Zhu, R., 2006. Magnetostratigraphic study of the Kuche Depression, Tarim Basin, and Cenozoic uplift of the Tian Shan Range, Western China. Earth Planet. Sci. Lett. 251, 346–364.

Huang, B.C., Piper, J.-D.A., Qiao, Q.Q., Wang, H.L., Zhang, C.X., 2010. Magnetostratigraphic and rock magnetic study of the Neogene upper Yaha section, Kuche Depression (Tarim Basin): implications to formation of the Xiyu conglomerate formation, NW China. J. Geophys. Res. 115, B01101 (doi: 1029/2008JB006175).

Ji, J.L., Luo, P., White, P., Jiang, H.C., Gao, L., Ding, Z.L., 2008. Episodic uplift of the Tianshan Mountains since the late Oligocene constrained by magnetostratigraphy of the Jingou River section, in the southern margin of the Junggar Basin, China. J. Geophys. Res. 113. http://dx.doi.org/10.1029/2007JB005064.

Jia, C.Z., Zhang, S.B., Wu, S.Z., 2004. Stratigraphy of the Tarim Basin and Adjacent Areas. Science Press, Beijing (1063 pp. (in Chinese)).

Jin, X., Wang, J., Chen, B., Ren, L., 2003. Cenozoic depositional sequences in the piedmont of the West Kunlun and their paleogeographic and tectonic implications. J. Asian Earth Sci. 21, 755–765.

Jin, Z.J., Yang, M.H., Lu, X.X., Sun, D.S., Tang, X., Peng, G.X., Lei, G.L., 2008. The tectonics and petroleum system of the Qiulitagh fold and thrust belt, northern Tarim basin, NW China. Mar. Pet. Geol. 25, 767–777.

Jolivet, M., Brunel, M., Seward, D., Xu, Z., Yang, J., Roger, F., Tapponnier, P., Malavieille, J., Arnaud, N., Wu, C., 2001. Mesozoic and Cenozoic tectonics of the northern edge of the Tibetan plateau: fission-track constraints. Tectonophysics 343 (1–2), 111–134.

Jolivet, M., Dominguez, S., Charreau, J., Chen, Y., Li, Y.A., Wang, Q.C., 2010. Mesozoic and Cenozoic tectonic history of the Central Chinese Tian Shan: reactivated tectonic structures and active deformation. Tectonics http://dx.doi.org/10.1029/2010TC002712.

Kent-Corson, M.L., Ritts, B.D., Zhuang, G.S., Bovet, P.M., Graham, S.A., Page Chamberlain, C., 2009. Stable isotopic constraints on the tectonic, topographic, and climatic evolution of the northern margin of the Tibetan Plateau. Earth Planet. Sci. Lett. 282 (1–4), 158–166.

Kirschvink, J.L., 1980. The least-square line and plane and the analysis of paleomagnetic data. Geophys. J. R. Astron. Soc. 62, 699–718.

Lan, X., 1997. Paleogene bivalve communities in the western Tarim Basin and their paleoenvironmental implications. Palaeoworld 7, 137–157.

Lan, X., Wei, J., 1995. Late Cretaceous–Early Tertiary Marine Bivalve Fauna from the Western Tarim Basin. Chinese Science Publishing House, Beijing (212 pp. (in Chinese)).

Li, Z., Song, W.J., Peng, S.T., Wang, D.X., Zhang, Z.P., 2004. Mesozoic–Cenozoic tectonic relationships between the Kuqa Subbasin and Tian Shan, northwest China: constraints from depositional records. Sediment. Geol. 172, 223–249.

Li, X.C., Wang, Y., Ding, X.Z., 2005. The age of Late Cenozoic molasse in the front of the western Kunlun Xinjiang and its significance. J. Geomech. 11 (2), 181–186 (in Chinese with English abstract).

Li, Y.J., Yang, G.X., Guo, W.J., Bi, M.B., Luan, X.D., Li, Z.C., Li, H., Tong, L.M., 2007. The disintegration and geological significance of the Kuoerku granite batholith in Awulale, western Tian Shan. Xinjiang Geol. 25 (3), 233–236 (in Chinese with English abstract).

Li, C.X., Dupont-Nivet, G., Guo, Z.J., 2011. Magnetostratigraphy of the Northern Tian Shan foreland, Taxi He section, China. Basin Res. 23 (1), 101–117.

Liao, L., Wang, B.Q., Cheng, X.G., Lei, G.L., Chen, H.L., Yao, Q., 2012. Cenozoic structural deformation of the thrusting zone and its control on hydrocarbon accumulation in northeastern Pamir. J. Chin. Univ. Min. Technol. 41 (5), 776–782.

Liu, H., Wang, G.C., Cao, K., Meng, Y.N., Wang, A., Zhang, K.X., 2010. The detrital zircon fission-track ages constraint to tectonic process in west Kunlun and adjacent regions. Front. Earth Sci. Chin. 17 (3), 64–78 (in Chinese with English abstract).

Lu, H.H., Douglas, W.B., Li, Y.L., Liu, Y.M., 2010. Late Cenozoic structural and stratigraphic evolution of the northern Chinese Tian Shan foreland. Basin Res. 22, 249–269.

Mao, S., Norris, G., 1988. Late Cretaceous–Early Tertiary Dinoflagellates and Acritarchs from the Kashi Area, Tarim Basin, Xinjiang Province, China. Royal Ontario Museum, Toronto.

Molnar, P., Tapponnier, P., 1975. Cenozoic tectonics of Asia: effects on a continental collision. Science 189, 419–426.

Patriat, P., Achache, J., 1984. India–Asia collision chronology has implications for crustal shortening and driving mechanism of plates. Nature 311, 615–621.

Pomazkov, K.D., 1972. Kyrgyz SSR geological description. USSR Geology. Publishing House 'NEWPA', Moscow.

Ramstein, G., Fluteau, F., Besse, J., Joussaume, S., 1997. Effect of orogeny, plate motion and land–sea distribution on Eurasian climate change over the past 30 million years. Nature 386, 788–795.

Şengör, A.M.C., Natal'in, B.A., Burtman, V.S., 1993. Evolution of the Altaid tectonic collage and Paleozoic crustal growth in Eurasia. Nature 364, 299–307. http://dx.doi.org/10.1038/364299a0.

Sobel, E.R., 1995. Basin Analysis and Apatite Fission Track Thermochronology of the Jurassic–Paleogene Southwestern Basin, NW China. (Ph.D. thesis). Stanford University, Stanford California.

Sobel, E.R., Dumitru, T.A., 1997. Exhumation of the margins of the western Tarim basin during the Himalayan orogeny. J. Geophys. Res. 102, 5043–5064.

Sobel, E.R., Chen, J., Heermance, R.V., 2006. Late Oligocene–Early Miocene initiation of shorting in the Southwestern Chinese Tian Shan: implications for Neogene shorting rate variations. Earth Planet. Sci. Lett. 247, 70–81.

Sobel, E.R., Schoenbohm, L.M., Chen, J., Thiede, R., Stockli, D.F., Sudo, M., Strecker, M.R., 2011. Late Miocene–Pliocene deceleration of dextral slip between Pamir and Tarim: implications for Pamir orogenesis. Earth Planet. Sci. Lett. 304, 369–378.

Sobel, E.R., Chen, J., Schoenbohm, L.M., Thiede, R., Stockli, D.F., Sudo, M., Strecker, M.R., 2013. Oceanic-style subduction controls late Cenozoic deformation of the Northern Pamir orogen. Earth Planet. Sci. Lett. 363, 204–218.

Sun, J.M., Zhu, R.X., Bowler, J., 2004. Timing of the Tianshan Mountains uplift constrained by magnetostratigraphic analysis of molasse deposits. Earth Planet. Lett. 219, 239–253.

Sun, J.M., Li, Y., Zhang, Z.Q., Fu, B.H., 2009. Magnetostratigraphic data on Neogene growth folding in the foreland basin of the southern Tianshan Mountains. Geol. Soc. Am. 37 (11), 1051–1054.

Tang, T., Yang, H., Lan, X., Yu, C., Xue, Y., Zhang, Y., Hu, L., Zhong, S., Wei, J., 1989. Marine Late Cretaceous and Early Tertiary Stratigraphy and Petroleum Geology in Western Tarim Basin, China. Science Press, Beijing.

Tapponnier, P., Molnar, P., 1977. Active faulting and tectonics in China. J. Geophys. Res. 82, 2905–2929.

Tapponnier, P., Xu, Z., Roger, F., Meyer, B., Arnaud, N., Wittlinger, G., Yang, J., 2001. Oblique, stepwise rise and growth of the Tibetan Plateau. Science 294 (5547), 1671–1677.

Tauxe, L., 1998. Paleomagnetic principles and practice. Modern Approaches in GeophysicsKluwer Academic Publisher, Dordrecht/Boston/London, p. 299.

Thomas, J.C., Chauvin, A., Gapias, D., Bazhenov, M.L., Perroud, H., Cobbold, P.R., Burtman, V.S., 1994. Paleomagnetic evidence for Cenozoic block rotations in the Tadjik depression (Central Asia). J. Geophys. Res. 99, 15141–15160.

Van Hinsbergen, D.J.J., Kapp, P., Dupont-Nivet, G., Lippert, P.C., DeCelles, P.G., Torsvik, T.H., 2011. Restoration of Cenozoic deformation in Asia and the size of Greater India. Tectonics 30. http://dx.doi.org/10.1029/2011tc002908 (TC5003).

Van Hinsbergen, D.J.J., Lippert, P.C., Dupont-Nivet, G., McQuarrie, N., Doubrovine, P.V., Spakman, W., Torsvik, T.H., 2012. Greater India Basin hypothesis and a two-stage Cenozoic collision between India and Asia. Proc. Natl. Acad. Sci. 109, 7659–7664.

Wang, J., Jin, X.C., Ren, L.D., Chen, B.W., 1999. Apatite fission track study of Cenozoic deposits of the Keliyang section, West Kunlun. Acta Geosci. Sin. 20, 159–164 (in Chinese with English abstract).

Wang, Y.B., Wang, Y., Liu, X., Fu, D.R., Wang, J., Wang, S.C., 2001. Apatite fission-track records of Mesozoic and Cenozoic episodic reactivation of the Tianshan and West Kunlun Mountains. Reg. Geol. Ser. China 20 (1), 94–99 (in Chinese with English abstract).

Wang, Y., Wang, Y.B., Liu, X., Xiao, X.C., 2002. Apatite fission-track ages of Late Cenozoic sediments from Kokyar section in western Kunlun foreland basin and their significance. Xinjiang Geol. 20, 43–46 (in Chinese with English abstract).

Wang, F., Zhou, X.H., Zhang, L.C., Ying, J.F., Zhang, Y.T., Wu, F.Y., Zhu, R.X., 2006. Late Mesozoic volcanism in the Great Xing'an range (NE China): timing and implications for the dynamic setting of NE Asia. Earth Planet. Sci. Lett. 251, 179–198.

Wang, Q.C., Li, S.J., Du, Z.L., 2009. Differential uplift of the Chinese Tian Shan since the Cretaceous: constraints from the sedimentary petrography and apatite fission-track dating. Int. J. Earth Sci. 98, 1341–1363.

Wang, L.N., Ji, J.Q., Sun, D.X., Xu, Q.Q., Tu, J.Y., Zhang, Z.C., Han, B.F., 2010. The uplift history of south-western Tianshan — implications from AFT analysis of detrital samples. Chin. J. Geophys. 53 (4), 931–945 (in Chinese with English abstract).

Wei, H.H., Meng, Q.R., Ding, L., Li, Z.Y., 2014. Tertiary evolution of the western Tarim Basin, northwest China: a tectonic-sedimentary response to northward indentation of the Pamir salient. Tectonics 32 (3), 558–575.

Windley, B.F., Alexeiev, D., Xiao, W., Kroner, A., Badarch, G., 2007. Tectonic models for accretion of the Central Asian Orogenic Belt. J. Geol. Soc. Lond. 164, 31–47.

Wu, C.D., Guo, Z.J., Fang, S.H., Zhang, Z.C., 2006. The Mesozoic filling sequences and controlling factors in the southern Junggar Basin. In: Guo, Z.J., Chen, Z.L., Shu, L.S., Li, S.X. (Eds.), Mesozoic–Cenozoic Intercontinental Orogeny and Mineralization of the Sandstone-type Uranium Deposit in the Central Asian Orogenic Belt, Northwest China. Geological Publishing House, Beijing, pp. 80–94 (in Chinese with English abstract).

Yang, Y., Liu, M., 2002. Cenozoic deformation of the Tarim plate and the implications for mountain building in the Tibetan Plateau and the Tian Shan. Tectonics 21, 1059. http://dx.doi.org/10.1029/2001TC001300.

Yang, H., Jiang, X., Lin, S., 1995. Late Cretaceous–Early Tertiary Ostracod Fauna from Western Tarim Basin, South Xinjiang, China. Science Press, Beijing.

Yang, W., Jolivet, M., Dupont-Nivet, G., Guo, Z.J., Zhang, Z.C., Wu, C.D., 2013. Source to sink relations between the Tian Shan Range and Junggar Basin (northwest China) from Late Paleozoic to Quaternary: evidence from detrital U–Pb zircon geochronology. Basin Res. 24, 1–22.

Yang, W., Jolivet, M., Dupont-Nivet, G., Guo, Z., 2014. Mesozoic–Cenozoic tectonic evolution of southwestern Tian Shan: evidence from detrital zircon U/Pb and apatite fission track ages of the Ulugqat area, Northwest China. Gondwana Res. 26 (3–4), 986–1008.

Yin, A., Nie, S., Craig, P., Harrison, T.M., 1998. Late Cenozoic tectonic evolution of the southern Chinese Tian Shan. Tectonics 17 (1), 1–27.

Yin, A., Rumelhart, P.E., Butler, R., Cowgill, E., Harrison, T.M., Foster, D.A., Ingersoll, R.V., Zhang, Q., Zhou, X.Q., Wang, X.F., Hanson, A., Raza, A., 2002. Tectonic history of the

Altyn Tagh fault system in northern Tibet inferred from Cenozoic sedimentation. Geol. Soc. Am. Bull. 114 (10), 1257–1295.
Zhang, Z.C., Guo, Z.J., Wu, C.D., Fang, S.H., 2007. Thermal history of the Jurassic strata in the Northern Tianshan and its geological significance, revealed by apatite fission-track and vitrinite-reflectance analysis. Acta Petrol. Sin. 23 (7), 1683–1695 (in Chinese with English abstract).
Zheng, J.J., He, X.X., Liu, S.W., 1999. Dictionary of Chinese Stratigraphy — Tertiary. Geology Press, Beijing (163 pp. (in Chinese)).
Zheng, H.B., Huang, X.T., Butcher, K., 2006. Lithostratigraphy, petrography and facies analysis of the Late Cenozoic sediments in the foreland basin of the West Kunlun. Palaeogeogr. Palaeoclimatol. Palaeoecol. 241, 61–78.